Observation of abundant heat production from a reactor device and of isotopic changes in the fuel

Giuseppe Levi
Bologna University, Bologna, Italy

Evelyn Foschi
Bologna, Italy

Bo Höistad, Roland Pettersson and Lars Tegnér
Uppsala University, Uppsala, Sweden

Hanno Essén
Royal Institute of Technology, Stockholm, Sweden

ABSTRACT

New results are presented from an extended experimental investigation of anomalous heat production in a special type of reactor tube operating at high temperatures. The reactor, named E-Cat, is charged with a small amount of hydrogen-loaded nickel powder plus some additives, mainly Lithium. The reaction is primarily initiated by heat from resistor coils around the reactor tube. Measurements of the radiated power from the reactor were performed with high-resolution thermal imaging cameras. The measurements of electrical power input were performed with a large bandwidth three-phase power analyzer. Data were collected during 32 days of running in March 2014. The reactor operating point was set to about 1260 ºC in the first half of the run, and at about 1400 °C in the second half. The measured energy balance between input and output heat yielded a COP factor of about 3.2 and 3.6 for the 1260 ºC and 1400 ºC runs, respectively. The total net energy obtained during the 32 days run was about 1.5 MWh. This amount of energy is far more than can be obtained from any known chemical sources in the small reactor volume.
A sample of the fuel was carefully examined with respect to its isotopic composition before the run and after the run, using several standard methods: XPS, EDS, SIMS, ICP-MS and ICP-AES. The isotope composition in Lithium and Nickel was found to agree with the natural composition before the run, while after the run it was found to have changed substantially. Nuclear reactions are therefore indicated to be present in the run process, which however is hard to reconcile with the fact that no radioactivity was detected outside the reactor during the run.

1. Introduction

This paper presents the results from a new extended study carried out on the "E-Cat" reactor, a device invented by Andrea Rossi. Various tests of this reactor have indicated that an excessive amount of heat is generated from a fuel consisting of hydrogen-loaded nickel powder plus some additives. The heat generating process is initiated by heat from resistor coils around the reactor tube. In addition, the resistor coils are fed with some specific electromagnetic pulses. The E-Cat reactor was tested in March 2013 by the same collaboration performing the present test and a report is given in ref. [1]. The March 2013 test showed indeed a clear indication that abnormal heat was generated, i.e. that the amount of heat could not be explained by any chemical processes in the limited volume of the reactor tube. This striking result prompted us to investigate this phenomenon further. Therefore a second test has now been performed, this time over a much longer period of time (32 days). Also, additional instrumentation was employed to further improve and secure the experimental conditions during the run. A longer test was also motivated to investigate the long term stability of the E-Cat operation, as well as running it at two different operational settings for comparison. Furthermore, and more importantly, we wanted to investigate if the nuclear composition of the fuel had changed due to the heat generating process. Such an investigation is indispensable in order to find out if the heat generating process has its origin in transformations at the nuclear level. A careful analysis of the fuel

isotope composition has therefore been performed on samples taken by us before and after the experimental run using the standard methods of SIMS, XPS, EDS and the chemical element analysis ICP-MS and ICP-AES.

In the course of the year following the previous tests, the E-Cat's technology was transferred to Industrial Heat LLC, United States, where it was replicated and improved. The present E-Cat reactor is therefore an improved version running at higher temperature than the one used in the March 2013 experiment. The general experimental procedure in the present test was the same as in the March test, i.e. the input power was carefully monitored with appropriate instruments, and the output power was determined by measuring the emitted radiation as well as calculating the heat dissipation from convection. The test started with a run with no fuel in the reactor in order to make sure that our experimental set-up gave a perfect balance between the measured input and output power.

Since we required that our measurements be carried out in an independent laboratory with our own equipment, the experiment was purposely set-up and hosted within an industrial establishment which was not in any way connected with Andrea Rossi's businesses or those of his partners. The test was thus performed in Barbengo (Lugano), Switzerland, in a laboratory placed at our disposal by Officine Ghidoni SA.

2. Reactor characteristics and experimental setup

The reactor investigated on this occasion is outwardly quite different from the ones used in the tests held in the past years. Its external appearance is that of an alumina cylinder, 2 cm in diameter and 20 cm in length, ending on both sides with two cylindrical alumina blocks (4 cm in diameter, 4 cm in length), non-detachable from the body of the reactor, which henceforth will be referred to as "caps". An image of the reactor is given in Figure1. Whereas the surface of the caps is smooth, the outer surface of the body of the E-Cat is molded in triangular ridges, 2.3 mm high and 3.2 mm wide at the base, covering the entire surface and designed to improve convective thermal exchange (cylinder diameter is calculated from the bases of the ridges). In this way, the current model of E-Cat is capable of attaining higher temperatures than the earlier models, avoiding internal melting, a previously fairly frequent occurrence [1].

Figure 1. Weighing the E-Cat after the test (452 g). The ridges along the body of the reactor increase the dissipation surface for natural heat convection. The power supply cables run through the two cylindrical extremities (termed "caps"), and were cut prior to weighing.

Three braided high-temperature grade Inconel cables exit from each of the two caps: these are the resistors wound in parallel non-overlapping coils inside the reactor. A thermocouple probe, inserted into one of the caps, allows the control system to manage power supply to the resistors by measuring the internal temperature of the reactor. The hole for the thermocouple probe is also the only access point for the fuel charge. The thermocouple probe cable is inserted in an alumina cement cylinder, which acts as a bushing and perfectly fits the hole, about 4 mm in diameter. When charging the reactor, the bushing is pulled out, and the charge is inserted. After the thermocouple probe has been lodged back in place, the bushing is sealed and secured with alumina cement. To extract the charge, pliers are used to open the seal.

The resistors and the copper cables of the three-phase power supply are connected outside the caps, in the classic delta configuration. For 50 cm from the reactor, the power cables are contained in hollow alumina rods (three per side), 3 cm in diameter (Figure 2). The purpose of the rods is to insulate the cables and protect the connections.

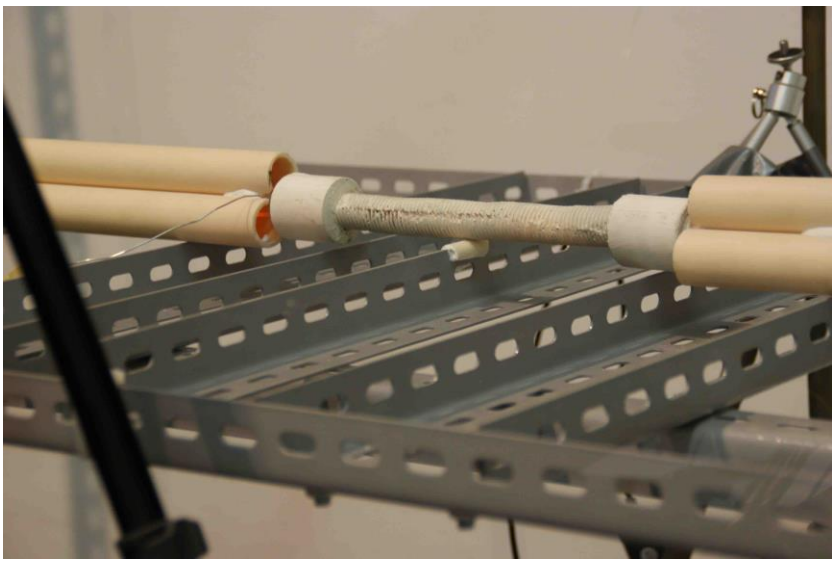

Figure 2.The E-Cat, installed on its metal frame. Note the two sets of three alumina rods (one per side) thermally and electrically insulating the supply cables that run through them. On the left, the cable connecting to the K-type probe may be seen. The strut under the center of the reactor has been covered with alumina cement, which provides thermal insulation of the reactor from the strut.

The E-Cat's control apparatus consists of a three-phase TRIAC power regulator, driven by a programmable microcontroller; its maximum nominal power consumption is 360 W. The regulator is driven by a potentiometer used to set the operating point (i.e. the current through the resistor coils, normally 40-50 Amps), and by the temperature read by the reactor's thermocouple.

Both the reactor and the rods lie on a metal frame, the points of contact with the frame being thermally insulated with alumina cement. The whole frame lies on an insulating rubber mat on the floor (Figure 3).

Figure 3. Experiment setup for the measurements. Foreground: reactor control system, the two PCEs for electric power measurements, and one of the multimeters used to verify that no DC components were present. Background: reactor, the two thermal imagery cameras. Note the 6 dosimeters (pairs of red and blue rectangles: 2 on wall, two to the left of reactor, and two to the right, on the far ends of the metal frame) for radiation emission measurements.

As in the previous tests, the calculation of the E-Cat's average power and energy production was performed by evaluating the power emitted both by radiation and convection. Our instruments consisted of two thermal imaging cameras to measure average surface temperatures, two power and harmonics analyzers for electrical consumption measurements, and three digital multimeters to measure any possible DC component in the power supply.

The cameras used were two Optris PI 160 Thermal Imagers, one provided with a 30° × 23° lens and 160 × 120 pixel UFPA sensors, capable of reading temperatures up to 900°C, the other with a 48° ×37° lens, capable of measuring temperatures up to 1500°C. The spectral range for both cameras is from 7.5 to 13 μm. The power analyzers were two PCE 830 units from PCE Instruments, capable of measuring, and displaying on an LCD display, electric current, voltage and power values, as well as the corresponding waveforms. These instruments are capable of reading voltage and AC current values up to 5 kHz.

The choice of instruments was warranted both by the straightforwardness of the experimental setup and the precision of the instruments themselves. Designing a calorimetric measurement by means of a cooling fluid would have been more complex, especially in the light of the high temperatures reached by the E-Cat.

All the instruments used during the test are property of the authors of the present paper, and were calibrated in their respective manufacturers' laboratories. Moreover, once in Lugano, a further check was made to ensure that the PCEs and the IR cameras were not yielding anomalous readings. For this purpose, before the official commencement of the test, both PCEs were individually connected to the power mains selected for powering the reactor. For each of the three phases, readings returned a value of 230 ± 2V, which is appropriate for an industrial establishment power network. The IR cameras, on the other hand, were focused on circular tabs of adhesive material of certified emissivity (henceforth referred to as "dots"). The relevant readings were compared to those obtained from a thermocouple used to measure ambient temperature, and were found to be consistent with the latter, the differences being < 1°C.

Throughout the test, all the above instruments were connected to the same computer, wherein all the acquired data was saved. For both the PCEs and the IR cameras, data acquisition frequency was set at 0.5 Hz.

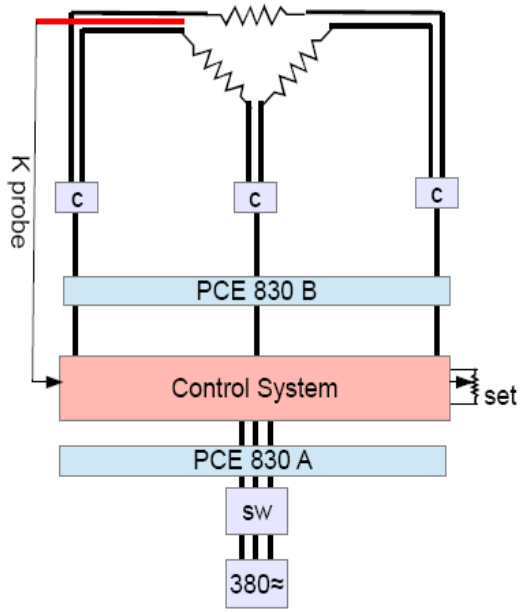

Figure 4.Wiring diagram. The two PCEs are located one upstream and one downstream from the control instruments, a TRIAC three-phase power regulator driven by a potentiometer and by the temperature read by the K-probe. The resistors are connected in delta configuration (SW = Switch, C = Connection Box). Note that, in the text, the three cables running from the control system to C are termed C_1, whereas the six cables running from C to the reactor are termed C_2.

Figure 4 details the electrical connections of all elements of the experimental setup. The two PCEs were inserted one upstream and one downstream of the control unit: the first allowed us to measure the current, voltage and power supplied to the system by the power mains; the second measured these same quantities as input to the reactor. Readings were consistent, showing the same current waveform; furthermore, they enabled us to measure the power consumption of the control system, which, at full capacity, was seen to be the same as the nominal value declared by the manufacturer.

Special attention was given to measuring the current and voltage input to the system: the absence of any DC component in the power supply was verified in various occasions in the course of the test, by means of digital multimeters and supplementary clamp ammeters. We also verified that all the harmonics of the waveforms input to the system were amply included in the range measurable by the PCEs (Figure 5). The three-phase current line supplying all the energy used for the test came from an electrical panel belonging to the establishment hosting our laboratory, to which further unrelated three-phase current equipment was connected.

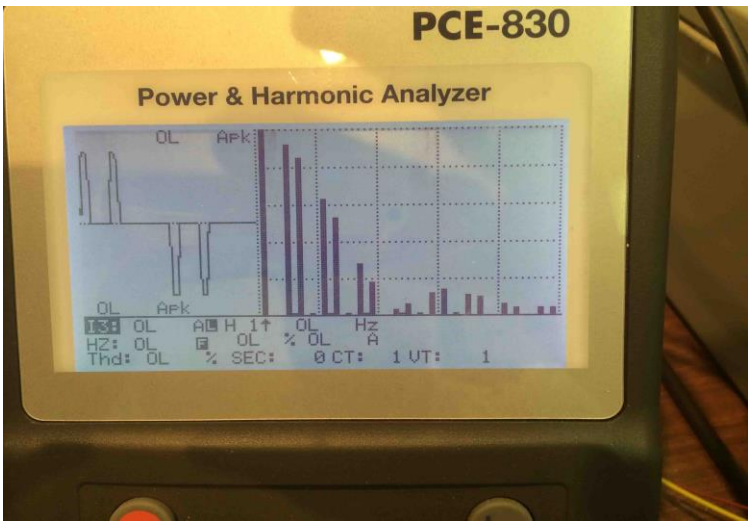

Figure 5.The PCE display downstream from the control unit. On the left, one can see the current's waveshape (identical in both PCEs), on the right its harmonics analysis. Note that the PCE is capable of correctly measuring up to 100 harmonics, though with diminishing precision. The figure reveals that all the most important harmonics are contained within the 20th harmonic, and, therefore, that all the wave shape harmonics input to the system lie within the PCE's measuring range.

David Bianchini, MSc and expert in radiation detection, was in charge of assessing possible ionizing radiation and neutrons emitted by the reactor charge, before, during and after operation. For this purpose, he provided the following instruments: a scintillation probe, a neutron radiation detector, a Geiger probe and various thermo luminescent dosimeters. For all types of radiation taken into consideration, background radiation was measured beforehand, both inside the laboratory where the test took place, and in various premises belonging to the establishment hosting us. Subsequently, Bianchini evaluated the possible presence of alpha, beta and gamma radiation by applying his instruments directly to the powder that was subsequently inserted into the reactor. The same operation was repeated after the end of the test on the powder extracted from the reactor. In both cases, no signs of activity were found. Similar readings were performed on the E-Cat, both during the dummy run without charge powder, and during normal operation. Several dosimeters located in the vicinity of the reactor were in operation during the entire 32 days of the test, for detecting neutron radiation. A detailed report on these operations and the results thereof is supplied as Appendix 1 to the present paper.

3. Experimental procedure

The first phase of the test was dedicated to measuring the "dummy reactor", i.e. the E-Cat operating without its internal charge. Conservation of energy dictates that all power supplied to the dummy reactor from the electric power line be dissipated as thermal energy to the environment by means of radiation and convection. Therefore, by comparing power input, as measured by the two power analyzers, to power output as measured by us, we were able to ascertain that no overestimation had occurred. In other words, the data relevant to the dummy reactor served the purpose of checking the method used. However, it was not meant to compare the operation of the loaded reactor to the dummy run. In fact, such a procedure would have required that the same amount of power be supplied to the dummy and to the reactor. Moreover, at the start of the measurements, there was no way of knowing what input power the loaded reactor would have absorbed. In fact, it is well known that some Inconel cables have a crystalline structure that is modified by temperature, and are capable of withstanding high currents only if they are operated at the appropriate temperature. If these conditions are not met, microscopic melt spots are liable to occur in the cables. So, there was some fear of fracturing the ceramic body, due to the lower temperature of the thermal generators

with respect to the loaded reactor. For these reasons, power to the dummy reactor was held at below 500 W, in order to avoid any possible damage to the apparatus.

The dummy reactor was switched on at 12:20 PM of 24 February 2014 by Andrea Rossi who gradually brought it to the power level requested by us. Rossi later intervened to switch off the dummy, and in the following subsequent operations on the E-Cat: charge insertion, reactor startup, reactor shutdown and powder charge extraction. Throughout the test, no further intervention or interference on his part occurred; moreover, all phases of the test were monitored directly by the collaboration.

"Dots" of known emissivity, necessary to subsequent data acquisition, were placed in various places on the cable rods. It was not possible to perform this operation on the dummy reactor itself (and *a fortiori* on the E-Cat), because the temperatures attained by the reactor were much greater than those sustainable by the dots. We also found that the ridges made thermal contact with any thermocouple probe placed on the outer surface of the reactor extremely critical, making any direct temperature measurement with the required precision impossible. Therefore, in the course of the test, we set the camera software to emissivity values valid for several alumina thermal ranges. However, in order to acquire from the literature a more adequate emissivity vs. temperature trend, it was necessary to know some of the characteristics of the material the reactor was made of, such as its composition and degree of purity. For this purpose, upon completion of the test, we took a sample of the material constituting the reactor; subsequently, Prof. Ennio Bonetti (Bologna) subjected it to X-Ray spectroscopy. The results confirmed that it was indeed alumina, with a purity of at least 99%. Details of this analysis will be found in Appendix 2.

After 23 hours' operation, the dummy reactor was switched off and disconnected from the power cables, to allow for one of the caps to be opened and the powder to be inserted. The powder had been previously placed in a small envelope, weighed (about 1 g), and then transferred to a test tube so that Bianchini could perform radioactivity measurements on it, after placing it in a low background lead well. Lastly, the contents of the test tube were poured inside the reactor, in the presence of a member of the experimental team. The leads were reconnected and the cap sealed with a mixture of water and alumina powder cement. The E-Cat was placed once again on its metal frame, and power was fed to it, the voltage being increased in progressive steps.

Upon completion of the gradual startup process procedure, the thermal camera indicated an average temperature for the body of the reactor of 1260°C, while the PCE recorded an electric power input to the E-Cat fluctuating at around 810 W. Although we had been informed that the E-Cat was capable of operating at higher power values, we had previously decided to keep to the lower value, and for almost 10 days no adjustments to the apparatus were made.

After this initial period, we noticed that the feedback system had gradually cut back the input current, which was yielding about 790 W. We therefore decided to increase the power, and set it slightly above 900 W. Thereby, we also obtained an important second measurement point. In a few minutes, the reactor body reached a temperature close to 1400°C. Subsequent calculation proved that increasing the input by roughly 100 watts had caused an increase of about 700 watts in power emitted. The speed with which the temperature had risen persuaded us to desist from any further attempt to increase the power input to the reactor. As we had no way of substituting the device in case of breakage or melting of internal parts, we decided to exercise caution and continue operating the reactor at ca. 900 W.

We also chose not to induce the ON/OFF power input mode used in the March 2013 test, despite the fact that we had been informed that the reactor was capable of operating under such conditions for as long a time as necessary. That power input mode, however, would have caused significant temperature increases during the brief intervals of time in which power was fed to the reactor. Moreover, the emissivity of alumina is temperature-dependent: this would have made all calculations troublesome and rendered analysis of the acquired data difficult.

In all the days that followed, no alterations were made to the instrumental apparatus or to the supply voltage. The dummy run was filmed and saved to a single thermography file; likewise, only one relevant file was produced by the PCE. But for the test on the E-Cat, we decided to save the data – both from the thermal camera constantly focused on the reactor body and from the PCE – on two-day intervals, yielding a total of 16 files from each instrument. This was done to avoid creating very large files, the accidental loss of which would have been inconvenient; moreover, it allowed us to perform preliminary analyses on the earliest data recorded. The other IR camera was primarily used to frame the hollow rods containing the power cables, and its position was changed often in the course of the test. When experimental conditions were seen to be constant, it would be pointed towards various parts of the reactor as well as of the rods, in order to verify the symmetry of heat emission and thus yield a more comprehensive picture of the thermal behavior of the system.

About 32 days from startup, on the 29 March 2014, at 11:40, the E-Cat was shut down, after gradually reducing its input power. The shutdown date had already been decided when organizing the test, and had nothing to do with the potential of the reactor, which was running normally. Therefore, no assumption may be made on the life of the powder charge, nor, consequently, on the total energy density of the reactor charge ,which means that the values found are only indicative of lower limits.

After cooling, the E-Cat was again opened by breaking one of the caps, and the powder was collected and put in a test tube. After Bianchini's readings, performed in a matter similar to those in the first phase, the test tube was handed back to us for further analysis, the results of which will presented in paragraph 8.

4. Data analysis method

4.1 Radiant power

Radiant power emitted both by the dummy reactor and by the E-Cat was calculated by means of the Stefan-Boltzmann formula:

$$M = \varepsilon\sigma T^4 \ [W/m^2] \qquad (1)$$

where ε is a parameter that assumes values ranging from 0 to 1, and represents the emissivity of a body, whereas σ is the Stefan-Boltzmann constant, the value of which is $5.67 \cdot 10^{-8}$ [W/m^2K^4].

Knowing the value of ε is of prime importance, both for the calculation of power emitted, and for reading temperatures with an IR camera, an instrument which does not measure the relevant parameter directly, but deduces it by means of a formula having several variables which must be supplied. Every thermal camera contains a detector where sensitive components generate an electric signal proportional to the IR radiation received. This signal is then amplified and processed by the device's electronics, and converted into an output signal proportional to the temperature of the object. This proportionality is expressed by an algorithm dependent on several parameters, such as the internal temperature of the detector (read directly by the camera sensors), ambient temperature, and the emissivity of the radiant body. The user sets the last two parameters before acquiring the data, but they may be also modified in the course of the analysis, because the camera software is capable of re-elaborating stored results and re-adapting them to new settings. For an in-depth description on how the cameras used by us work, see [2].

From the analyses performed on the sample taken from the reactor, we determined that the material constituting the outer shell is 99% pure alumina (Appendix 2); better yet, that impurities, if present, are below the experimental limit of measurement. We therefore retrieved from the literature [3] a discrete-point plot of the emissivity of said material as a function of temperature (Figure 6), and extracted from it the values necessary to reproduce the trend as a continuous line (Plot 1).

The error associated with the plot's trend has been measured at ± 0.01 for each value of emissivity: this uncertainty has been taken into account when calculating radiant energy.

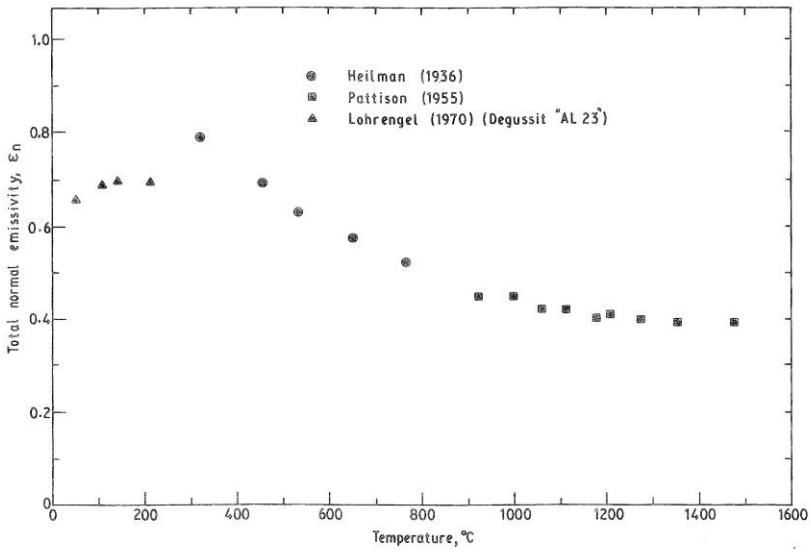

Figure 6.Trend of alumina emissivity vs. temperature; from [3].

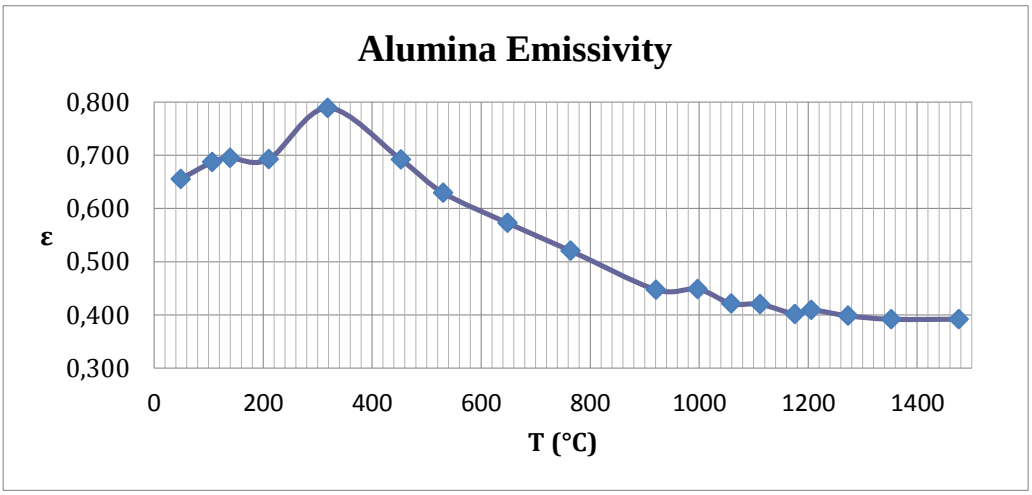

Plot 1. Alumina emissivity trend as a function of temperature, reproduced from data extracted from the plot in Figure 6 [3].

During the data analysis, in order to account for the several values of ε and the, at times, uneven distribution of heat, each thermography file was divided in an appropriate number of areas, to which the Stefan-Boltzmann formula was applied. The values for ε relevant to each area were assigned recursively, by correcting the settings until the same matching between temperature and emissivity indicated by Plot 1 was achieved. Iterative methods for determining the emissivity of an observed object are well known in the literature: some examples may be found in [4], [5].

It was not possible to extract any sample of the material constituting the rods, as this is firmer than that of the reactor. The rods were made of pure alumina, crystallized however with a different degree of fineness due to the industrial origin of their manufacture.

We therefore took the same emissivity trend found in the literature as reference; but, by applying emissivity reference dots along the rods, we were able to adapt that curve to this specific type of alumina, by directly measuring local emissivity in places close to the reference dots (Figure 7).

An example of all these procedures will be given in detail only for the dummy reactor, in paragraph 5.

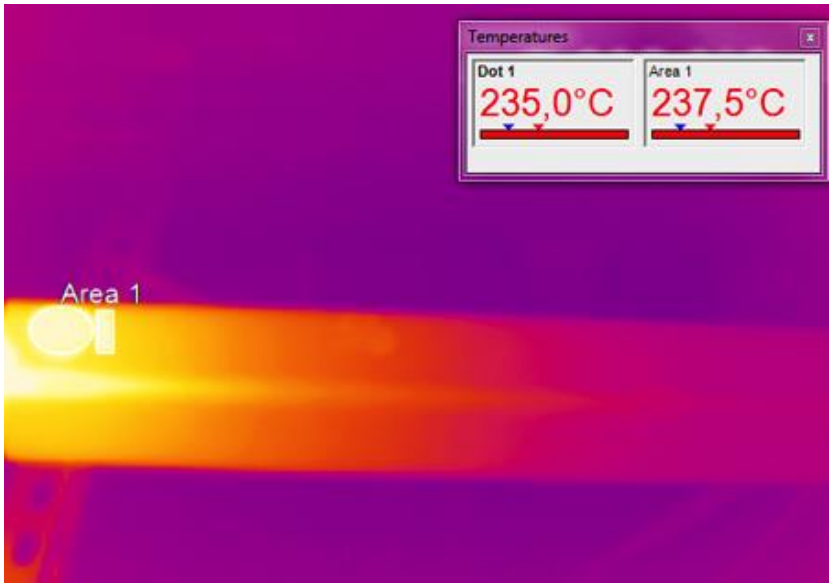

Figure 7. Detail of a thermography image of the rods to the right of the E-Cat. The circular bright spot is a reference "dot" (TiO_2 on Kapton film) which has higher emissivity (0.95) than that of alumina, and thus appears to be hotter. The temperature read on this dot (235°C) is the actual temperature of the tube. The temperature at the rectangle next to the circle (237.5 °C) is obtained by setting an emissivity value for alumina found in the literature [3.] The difference lies within the errors associated to the measurements.

4.2 Convection

In order to calculate the heat dissipated by convection, two different kinds of surfaces must be taken into consideration, the smooth cylindrical surfaces of the rods and reactor caps, and the ridged cylinder of the reactor body.

If one identifies both the rods and the reactor caps as cylinders immersed in air, one may, for each of them, calculate the heat Q emitted by convection per time unit by means of Newton's relation. If T_a indicates air temperature, A the surface area of a cylinder, and T_s the cylinder's temperature, we have:

$$Q = hA(T_s - T_a) = hA\Delta T \text{ [W]} \quad (2)$$

where h defines the thermal exchange coefficient [W/m²K].

Calculating h is the fundamental problem of thermal convection calculation, and has been tackled by various authors more or less empirically (See f.i. [6], [7], and [8]). In the specific case of cylindrical surfaces, one of the more commonly used expressions is the following one:

$$h = (kCRa^n) / D \text{ [W/m²K]} \quad (3)$$

where k indicates the coefficient of thermal conductivity of air [W/mK], C and n are two constants, Ra is Rayleigh's number, and D the diameter of the cylinder. Rayleigh's number is a dimensionless parameter given by the following expression:

$$Ra = (g\beta(T_s - T_a)D^3) / \nu\alpha \quad (4)$$

where g [m/s^2] is gravitational acceleration, $\beta[K^{-1}]$ is the volumetric thermal expansion coefficient, which, for an ideal gas (applied here to air for simplicity) is= 1/T; next, ν [m²/s] is kinematic viscosity, and α [m²/s] is thermal diffusivity. Coefficients β, k, α, and ν are all temperature-dependent, and must be calculated at the so-called "film temperature" $T_f = (T_s + T_a) / 2$. Plots 2, 3, and 4 express these trends for a range of temperatures from 100 to 1000 K and have been taken from the data reported in Appendix A of [9].

Plot 2.

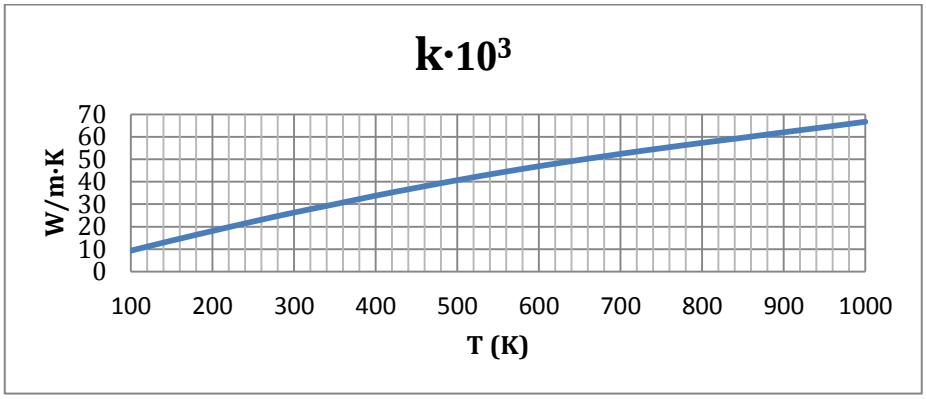

Plot 3.

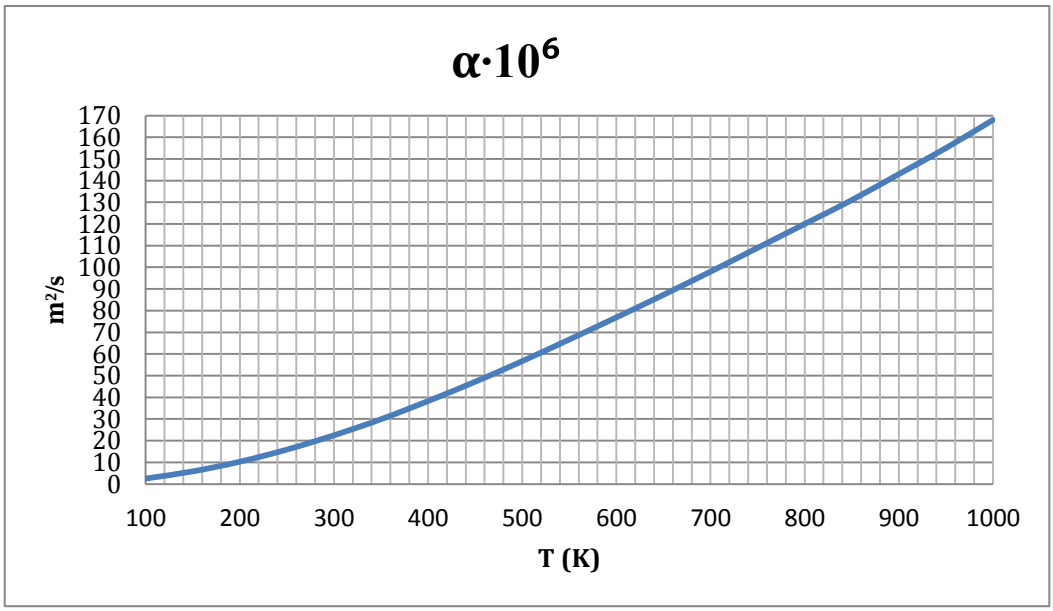

Plot 4.

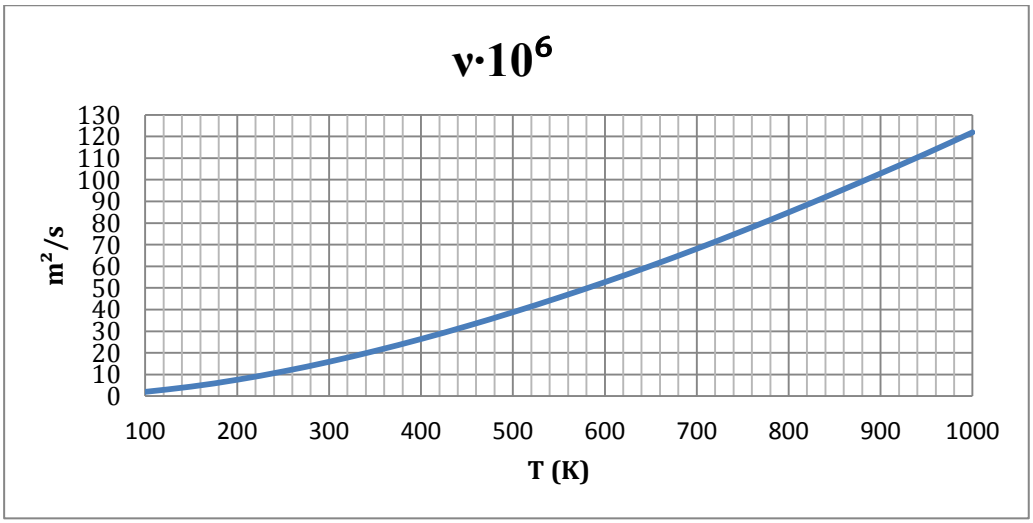

Plots 2, 3, and 4. Trends of thermal conductivity k [W/mK], kinematic viscosity ν [m²/s], and thermal diffusivity α [m²/s] of air in function of temperature, reproduced from data found in the literature [9]. The convention used to present numerical values of the properties is illustrated by this example: for T = 300 [K] we have $k \cdot 10^3 = 26.3$ [W/mK], $\nu \cdot 10^6 = 15.9$ [m²/s], and $\alpha \cdot 10^6 = 22.5$ [m²/s]; therefore k = 0.026 [W/mK], ν = 0.000016 and α = 0.000023.

The Rayleigh number expresses the ratio of buoyancy forces to viscous forces, and its value is indicative of the laminar-turbulent transition, which occurs when Ra $>10^9$. Constants C and n are dependent on the value of Ra, according to what is expressed by Table 1 [9].

Ra	C	n
10^{-10}-10^{-2}	0.675	0.058
10^{-2}-10^{2}	1.020	0.148
10^{2}-10^{4}	0.850	0.188
10^{4}-10^{7}	0.480	0.250
10^{7}-10^{12}	0.125	0.333

Table 1. Values of the constants C and n corresponding to variations of the Rayleigh number.

Thermal flow emitted by the body of the reactor by natural convection may be in turn calculated by an expression suitable to objects having circular fins, to which our ridges may be compared for simplicity's sake. Figure 8 shows a single circular fin, triangular in profile. This shape is the closest possible to the reactor's ridges, and is appropriate to represent them.

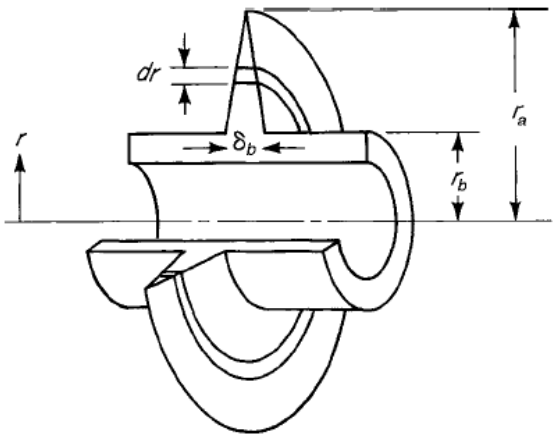

Figure 8. Representation of a circular fin having triangular profile. Its shape is very similar to that of the reactor ridges, and was used as a model to calculate natural convection.

Let us then approximate the body of the reactor to that of a cylinder having N fins, each one having surface A_f. If we take A_t as the its total surface, we have:

$$A_t = NA_f \quad (5)$$

The length of the reactor body is given by L = 200 mm, and that of the base of each ridge is given by δ_b = 3.25 mm. If we compare this to a finned cylinder having no space between fins, the number of ridges/fins along it is = N = L / $\delta_b \approx 61$. For the area of each fin, we have:

$$A_f = 2\pi(r_a^2 - r_b^2) = 3.22 \cdot 10^{-4}[m^2] \quad (6)$$

where r_a is the distance between the axis of the cylinder and the tip of a fin, = $1.23 \cdot 10^{-2}$[m], while r_b is the radius of the cylinder = $1.0 \cdot 10^{-2}$[m] (Figure 8). Note how this formula for the area is actually fit for fins

having a rectangular, not triangular, profile; this approximation is however commonly used, as one may see f.i.in [10].

We may calculate the total thermal power emitted by convection by the reactor body in the following manner [9]:

$$Q = N\eta h A_f (T_s - T_a) \text{ [W]} \quad (7)$$

assuming that coefficient h is equivalent of what one would have for a finless surface.

This coefficient is therefore calculated as in (3), referring to a cylinder having the size of the reactor but completely devoid of fins (see here [9]). Parameter η represents here the efficiency of each fin, and is an index of its thermal performance. Since the driving potential for convection is expressed by the difference in temperatures between a body and its exchange fluid, it is obvious that the maximum thermal flow for a fin would be had if its entire surface were at the same temperature as its base. However, as each fin is characterized by a finite resistance to thermal conduction, there will always be a thermal gradient along it, and the condition given above is a mere idealization. Therefore, the efficiency for a fin is defined as the ratio of heat actually exchanged with air to its the maximum ideal amount. In the case of a fin having triangular profile, one may calculate the trend of η as a function of a dimensionless parameter m, equal to:

$m = b(2h / k\delta_b)^{0.5}$ with $b = r_a - r_b = 2.3 \cdot 10^{-3}$ [m]; *k* [W/mK]: thermal conductivity of the cylinder (8)

This trend may be seen in Figure 9; for calculation details see [10].

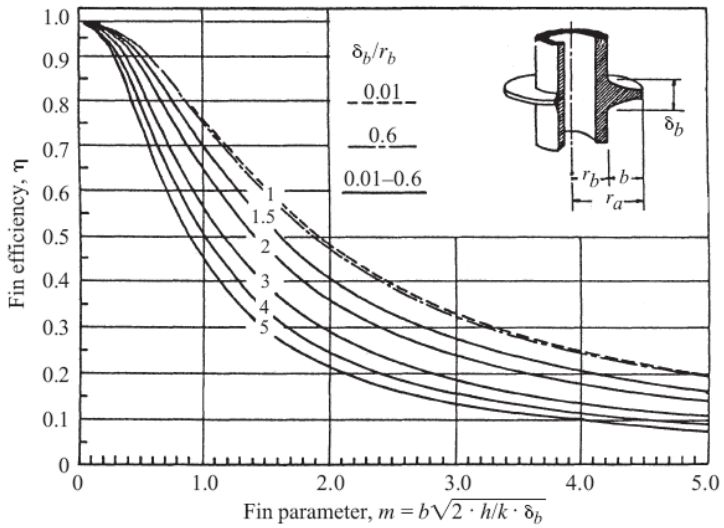

Figure 9. A plot showing the efficiency of a circular fin having triangular profile. From [10].

4.3 Joule heating in the cables

The cables supplying power to the reactor are made of copper and are several meters long. In the present run of the E-Cat the current flow may actually be higher than 40 A. For this reason, it is expedient to evaluate what portion of the current, fed to the system by the power mains, is dissipated by the cables as Joule heat. Figure 4 shows the cable layout from mains to load: three copper cables exit the power regulator, one for each phase, three meters in length each, with a cross-profile of 12.00 mm^2. In order to allow the delta configuration connection of the resistors, each of these cables is connected to another two cables, 2 m in length each, having a cross-section of 12.45 mm^2.

Given that the resistivity of copper is = 0.0175 Ω / m mm^2, one may easily deduce that the electrical resistance of the three cables exiting the regulator (Circuit 1, C_1) is = $R_1 = 4.375 \cdot 10^{-3}$ Ω, whereas that of the cables splitting off from these (Circuit 2, C_2) is = $R_2 = 2.811 \cdot 10^{-3}$Ω.

We may calculate the dissipated heat to the limited extent of the dummy reactor: the results relevant to the E-Cat will be given in Table 7, due to the fact that the average current values changed from day to day.

Measurements performed during the dummy run with the PCE and ammeter clamps allowed us to measure an average current, for each of the three C_1 cables, of I_1 = 19.7A, and, for each C_2 cable, a current of $I_1 / 2 = I_2$ = 9.85 A. The evaluation of heat dissipated by the first circuit is:

$$W_{C1} = 3(R_1 I_1^2) = 3(4.375 \cdot 10^{-3} \cdot (19.7)^2) = 5.1 \text{ [W]} \quad (9)$$

For the second circuit we have:

$$W_{C2} = 6(R_2 I_2^2) = 6(2.811 \cdot 10^{-3} \cdot (9.85)^2) = 1.6 \text{ [W]} \quad (10)$$

By adding the results, we have the total thermal power dissipated by the entire wiring of the dummy.

$$W_{tot.dummy} = 5.1 + 1.6 = 6.7 \approx 7 \text{[W]} \quad (11)$$

In the calculations that follow, relevant to the dummy reactor and the E-Cat's power production and consumption, the watts dissipated by Joule heating will be subtracted from the power supply values.

Note that the copper cables, 12.45 mm^2 in cross section, run through most of the six alumina rods, inside of which they are joined by a connecting terminal to the Inconel cables coming from the reactor. The length of Inconel cable inside the rods is but a few centimeters long. Therefore, if one considers that the copper cables run through almost the whole length of the rods (50 cm), it is possible to calculate what fraction of the 7 W given by (11) is emitted within the six rods themselves. For each of the six 50 cm lengths of copper cable, the relevant resistance is $7.028 \cdot 10^{-4}$Ω. From (10) we see that the heat dissipated inside the rods by the copper cables is = $6 \cdot (7.028 \cdot 10^{-4} \cdot (9.85)^2)$ = 0.4 W, that is to say, about 6% of the heat emitted by all the copper cables together. It is obvious that the heat emitted by the rods (which shall be calculated in detail in the next paragraph) is only in the least part generated by the cables running through them: on the contrary, that heat originates almost exclusively from the reactor, which, by conduction through the short lengths of Inconel cables coming from the caps, transmits it to the rods.

5. Analysis of data obtained from the dummy reactor

In order to determine the radiated and convection heat emitted by the dummy reactor, one must first of all find its surface temperature.

Figure 10 shows an image taken from the dummy's thermography file, processed for data analysis. Each cap has been divided into three parts, while the central body of the reactor has been divided into 10 parts. For each part, the measurements are as follows:

$$\text{Caps: } (2\pi \cdot R_{cap} \cdot L_{cap}) / 3 = 1.67 \cdot 10^{-3} m^2 \quad (12)$$

$$\text{Dummy reactor body: } (2\pi \cdot R_{reactor} \cdot L_{reactor}) / 10 = 1.25 \cdot 10^{-3} m^2 \quad (13)$$

where R indicates tap radius in (12) and reactor body radius in (13). L indicates the relevant lengths; for the reactor, the radius is that of the body without the ridges.

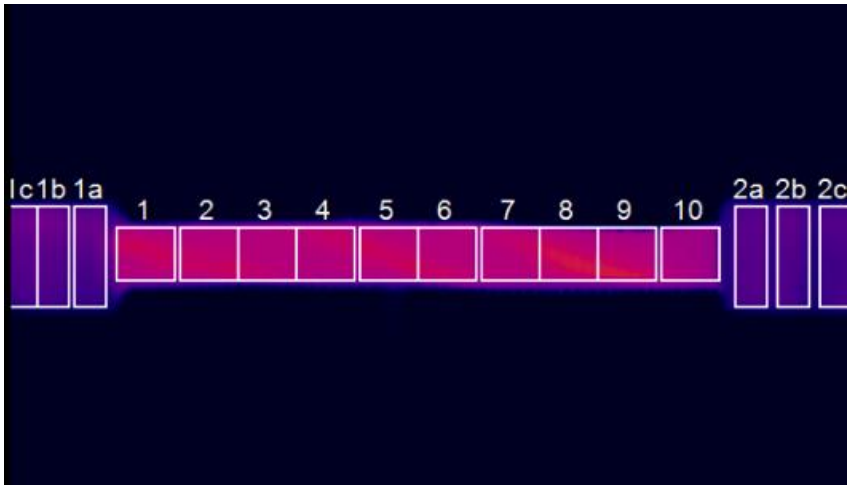

Figure 10. Detail of a thermography image from the dummy reactor run. The image was divided into several areas; the most appropriate emissivity settings were applied to each area.

An emissivity value has been assigned to each area, recursively calculated on the basis of the trend in Plot 1. The method applied for assigning the values is set forth in Tables 2a and 2b, by using as an example the results of a randomly chosen area, in our case Area No. 5, at a randomly chosen instant.

Table 2a

ε assigned	T obtained (°C)	ε for T obtained
1.00 →	366.6 →	0.76
0.76 →	426.6 →	0.71
0.71 →	443.1 →	0.69
0.69 →	450.3 →	0.69

Table 2b

ε assigned	T obtained (°C)	ε for T obtained
0.5 →	541.2 →	0.62
0.62 →	478.3 →	0.68
0.68 →	454.0 →	0.69
0.69 →	450.3 →	0.69

Tables 2a, 2b. Examples of values recursively assigned to emissivity. In the first table, the initial value is set at 1.00, whereas in the second table it is set at 0.5. In both cases, one sees that the correct emissivity assigned to Area 5 is 0.69. This proves that the method adopted here is independent of the starting value assigned to ε.

The IR camera was recording past the initial moments during which the dummy reactor was heating up, and up to a point at which it was operating at normal capacity. The file run was then stopped, and an emissivity reference value of 1 was set for each area. As one may see in the first table, for the instant chosen, the mean temperature of Area 5 indicated by the thermal camera's software is = 366.6°C for ε = 1. From the curve (ε vs. T), one can see that, for that mean temperature, the correct emissivity value would be 0.76; the next step is therefore changing the emissivity of area 5 according to this new value. We thus get a new estimate for the mean temperature of the area as 426.6°C, for which, according to the emissivity curve, one should have ε = 0.71. This procedure is continued until one gets a correct matching between emissivity and temperature, which — in the above case of area 5 —yields ε = 0.69 and T = 450.3°C. In order to prove that this method does not depend on the initial emissivity value chosen, Table 2b shows what happens when the initial value of ε has been nominally set at 0.5. As one may see, after a certain number of iterations, the same final result is found. After establishing what emissivity value settings were to be used for each area, we extracted the

temperatures relevant to all the 23 hours of the dummy run, and averaged them, obtaining a single final value for each one of them (for Area 5, this was = 450.3°C). This method was applied to all the areas of the dummy reactor, as well as to the rods and to the E-Cat, as we shall see.

A possible source of error in the calculation of the mean temperatures (and, consequently, in that of emitted power) must be seen in the uncertainty with which one reads the values of curve (ε vs. T). This uncertainty, valued at ± 0.01, was used to calculate the error to be associated with each result. In the case of area 5, for instance, all calculations were first performed for ε = 0.69, then for ε = 0.68 (i.e. ε = 0.69 –0.01), and finally for ε = 0.70 (i.e. ε = 0.69 + 0.01). The difference between the results obtained in the last two cases, compared to the first result, is the percentage error sought. In this manner, temperature fluctuations in each area with time, for which one would have to constantly reset emissivity, are also taken into account.

The maximum value reached by area 5 during the whole measurement was equal to 469°C, which would correspond to ε = 0.68, whereas the minimum value was equal to 443°C, which would warrant ε = 0.69.

After reckoning the average temperatures for each area, we calculated the watts emitted by radiation and convection for each area, and upon adding these, arrived at the total power dissipated by the dummy reactor. More specifically, for each area of the cap and of the reactor body, radiation values were obtained by applying equation (1) and subtracting from the result the contribution due to ambient temperature, which during the dummy test was 21°C (ε = 0.64). Using once again Area 5 as an example and expressing all temperatures in degrees Kelvin, as the formulas require, we get, for radiation:

$(\varepsilon \cdot T^4 – \varepsilon_{amb} \cdot T_{amb}^4) \cdot \sigma \cdot$ Area =

$= (0.69 \cdot (454.3 + 273.16)^4 – 0.64 \cdot (21 + 273.16)^4) \cdot 5.67 \cdot 10^{-8} \cdot 1.25 \cdot 10^{-3} = 13.4$ [W] (14)

For convection, we applied (2) to each area relevant to the reactor caps, and (7) to each area attributed to the reactor body. Taking Area 5 as an example, we must first calculate the heat exchange coefficient h, starting from the value assumed in this case by the Rayleigh number:

$Ra = (g\beta(T_s – T_a)D^3) / \nu\alpha = 28184.32$ (15)

($g = 9.8$ [m/s²], $\beta = 1 / T_f = 19 \cdot 10^{-4}$ [K^{-1}], $T_s = 727.19$[K], $T_a = 294$[K], $D = 0.02$[m], $\nu = 40 \cdot 10^{-6}$ [m²/s], $\alpha = 59 \cdot 10^{-6}$ [m²/s])

From Table 1 we can see that, for this value of Ra, we have: C = 0.48 and n = 0.25.

By (3) we then have:

$h = (kCRa^n) / D = 12.75$ [W/mK] (16)

where the thermal conductivity of air k is = $41 \cdot 10^{-3}$ [W/mK].

Coefficients k, ν, and α were calculated by means of Plots 2, 3, and 4, at a film temperature $T_f = 510.60$ K.

Furthermore, for each area of the body we know that the length L is 0.02 [m], that the number of fins is N ≈ 6, whereas r_b and δ_b (Figure 10) keep their previously established values (10^{-2} [m] and $3.2 \cdot 10^{-3}$ [m]).

In order to get the watts emitted by Area 5, one more parameter is lacking, namely fin/ridge efficiency, for which we need another parameter, m, given by (8). This last parameter depends on the thermal conductivity of alumina, which is, in turn, a function of its temperature. From [3] we learn that at the average temperature of Area 5 ($T_s = 727.19$[K]), *k* is ca. 10 [W/mK], therefore:

$m = b(2h / k\delta_b)^{0.5} = 0.065$ (17)

From Figure 9 we can see that for this value of m, the value of η is very close to 1 (≈ 0.98), which is to be expected, given the definition of efficiency and how it relates to the fairly small size of the ridges.

Now we can finally substitute all the values found in (7) and calculate heat emitted by convection by Area 5:

$Q = N\eta h A_f(T_s – T_a) = 10.46$ [W] (18)

For each cap, we applied (2), to each of the three areas attributed to each cap ($A = 16.7 \cdot 10^{-4}$ [m²], D = 0.04 [m]). For instance, for cap Area 1a, by consulting Plots 2, 3, and 4, and taking into account $T_f = 453.05$ [K], we get the following values: $k = 37 \cdot 10^{-3}$ [W/mK], $\nu = 32 \cdot 10^{-6}$ [m²/s] and $\alpha = 47 \cdot 10^{-6}$ [m²/s]. In this case, the Rayleigh number and coefficient h become:

$$Ra = (g\beta(T_s - T_a)D^3) / \nu\alpha = 292803.67 \quad (19)$$

$$h = (kCRa^n) / D = 10.33 \text{ [W/m²K]} \quad (20)$$

Heat emitted by convection by cap Area 1a alone is thus:

$$Q = hA(T_s - T_a) = 5.50 \text{ [W]} \quad (21)$$

Table 3 below shows, for each area, the values obtained for average temperature, power emitted by radiation, and power emitted by convection, when the appropriate emissivity is assigned; the last four columns give only the results relevant to the sum total of watts emitted by radiation and convection when emissivity is made higher or lower by uncertainty.

	ε	Average T (°C)	Radiation (W)	Convection (W)	TOT. (W)	ε – 0.01	TOT. (W)	ε + 0.01	TOT. (W)
Area 1	0.69	451.00	13.18	10.37	23.55	0.68	23.73	0.70	23.37
Area 2	0.69	449.93	13.10	10.34	23.44	0.68	23.62	0.70	23.27
Area 3	0.71	436.14	12.46	9.96	22.43	0.70	22.59	0.72	22.39
Area 4	0.71	435.88	12.44	9.96	22.40	0.70	22.57	0.72	22.36
Area 5	0.69	454.03	13.41	10.46	23.86	0.68	24.05	0.70	23.68
Area 6	0.71	443.31	12.99	10.16	23.15	0.70	23.32	0.72	22.98
Area 7	0.71	437.98	12.60	10.01	22.61	0.70	22.78	0.72	22.45
Area 8	0.69	461.64	13.99	10.67	24.66	0.68	24.85	0.70	24.47
Area 9	0.69	452.66	13.30	10.42	23.72	0.68	23.91	0.70	23.54
Area 10	0.73	412.90	11.18	9.44	20.62	0.72	20.77	0.74	20.48
Cap 1a	0.79	338.94	10.07	5.50	15.57	0.78	15.64	0.80	15.50
Cap 1b	0.79	323.63	9.05	5.20	14.25	0.78	14.31	0.80	14.18
Cap 1c	0.79	330.38	9.49	5.33	14.82	0.78	14.89	0.80	14.75
Cap 2a	0.79	319.85	8.81	5.12	13.93	0.78	14.00	0.80	13.87
Cap 2b	0.79	323.57	9.05	5.19	14.24	0.78	14.31	0.80	14.18
Cap 2c	0.79	311.31	8.29	4.95	13.24	0.78	13.30	0.80	13.18
TOTAL			183.41	133.09	316.50		318.65		314.67

Table 3. For each one of the areas that the caps and the body of the dummy reactor have been divided into, the table shows, subsequently: actual emissivity value, average temperature, power emitted by radiation, power emitted by convection, the sum of the last two values, emissivity minus uncertainty, the sum total of watts emitted if one sets “emissivity minus uncertainty”, emissivity plus uncertainty, and the sum total of watts if one sets “emissivity plus uncertainty”.

The total power emitted by the dummy reactor is 316.50 W, and the percentage error to be associated to this value is:

$$(318.65 – 314.67) / 316.50 = 0.0126 = 1.26\% \approx 1.3\% \quad (22)$$

The very same process used for the dummy reactor body was used to calculate the power emitted through radiation and convection by the rods. During the test, the rods were heated by conduction, from their being in contact with the reactor, and from the heat yielded to them by the lengths of Inconel cable external to the caps. Not only do the cables dissipate heat by Joule heating, they also subtract it from the reactor by conduction. Here too, the thermal images of each rod were divided into 10 areas. Because the rods were placed in overlapping positions, each one of them was capable of dissipating heat to the environment for only 2/3 of its surface; moreover, whereas the temperature of the two lower rods was more or less the same, the upper rod always indicated higher temperatures. For this reason, we decided to perform calculations on a thermography file corresponding to a side view, in which only one upper and one lower rod were visible, and to attribute to the third rod which was not framed by the camera the same values of the lower visible rod (Figure 11). Lastly, we found that the three rods connected to the cap on the right of the dummy reactor indicated slightly higher temperatures than those connected to the cap on the left, and that this difference was within the associated error margin. We therefore decided to perform the calculations for only one set of three rods (the cooler ones) and multiply the result by a factor of 2.

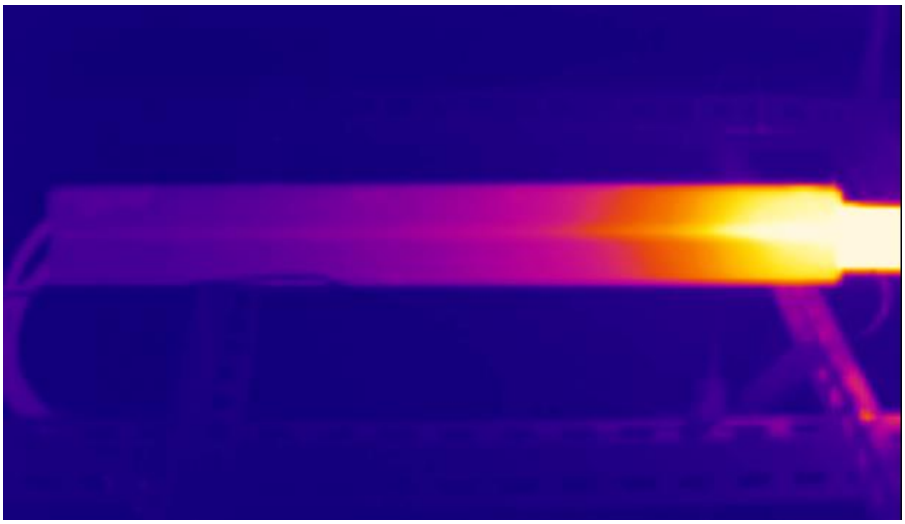

Figure 11.Thermography image of the set of three rods on the left of the reactor. To the third rod hidden behind the other two, we attributed the temperatures appropriate to the lower rod.

The dimensions of each area are given by:

$$(2\pi \cdot R_{rod} \cdot L_{rod}) / 10 = 4.71 \cdot 10^{-3} m^2 \quad (23)$$

where R and L are the radius and the length of each rod, respectively.

To each area, formulas (14) for calculating radiation and formula (18) convection were applied, substituting the appropriate values.

Table 4 shows all the results obtained for the areas of the upper rod (indicated by $_u$) and one of the lower rods (indicated by $_d$) of a set of three rods. In the columns from left to right, the first values found are relevant to the upper rod (subsequently: emissivity, average temperature, radiation power, convection power, and the sum of the last two values), followed by the values relevant to the lower rod. The sum of the results obtained for each area appears in the last line. Finally, the bottom cell of the last column of the table records

the watts emitted by one entire set of three rods, a value obtained by adding the total watts produced by the upper rod, to the total watts, multiplied by two, produced by the lower rod.

Area	ε_u	$T._u$(°C)	$Rad._u$ (W)	$Conv._u$(W)	$Tot._u$ (W)	ε_d	$T._d$ (°C)	$Rad._d$ (W)	$Conv._d$ (W)	$Tot._d$ (W)	Tot. 3 rods (W)
1	0.69	151.52	4.71	5.84	10.55	0.69	147.98	4.52	5.65	10.17	
2	0.69	125.13	3.36	4.45	7.81	0.69	118.89	3.07	4.13	7.20	
3	0.68	90.85	1.91	2.81	4.72	0.68	87.71	1.80	2.66	4.46	
4	0.67	68.17	1.15	1.72	2.87	0.67	68.15	1.15	1.72	2.87	
5	0.66	58.26	0.85	1.28	2.13	0.66	58.21	0.85	1.28	2.13	
6	0.66	54.12	0.74	1.11	1.85	0.66	52.82	0.71	1.06	1.77	
7	0.66	46.33	0.56	0.80	1.36	0.66	45.06	0.53	0.75	1.28	
8	0.66	40.02	0.42	0.56	0.98	0.66	38.89	0.39	0.52	0.91	
9	0.66	35.34	0.32	0.40	0.72	0.66	34.30	0.30	0.36	0.66	
10	0.66	31.82	0.25	0.28	0.53	0.66	31.09	0.23	0.26	0.49	
TOT.					33.52					31.94	97.4

Table 4. The values in the table refer to one of the two sets of three dummy reactor rods. Subscript "u" refers to the uppermost rod of the set, subscript "d" to one of the two lower rods (the same results apply to the second lower rod). Each rod has been divided into 10 areas. For each area, the table indicates, subsequently: assigned emissivity, average temperature, power emitted by radiation, power emitted by convection, the sum of the last two values. The last cell of the table gives the total watts emitted by one whole set of three rods, reckoned by multiplying the results relevant to the lower rod by 2, and adding them to those of the upper rod.

We can now calculate the total heat emitted from both sets of three rods, bearing in mind how much of their surface is actually emitting heat, and the associated error percentage (estimated at ca. 5%):

$$(97.40 \cdot 2/3) \cdot 2 = 129.86 \pm 5\% \text{ [W]} \quad (24)$$

In the previous paragraph, we have seen that the copper cables running through the rods emit a total of 0.4 W through Joule heating. This value should be subtracted from (24) because, contrary to the power calculated with that equation, it does not derive from heat generated by the reactor and transmitted to the rods by conduction, but from electric power supplied by the mains. However, as it is a very small value, it may be considered part of the error associated to (24).

Note also that part of the power produced by the rods is also due to Joule heat emitted by the short lengths of Inconel resistors connected to the copper cables inside the rods after leaving the caps. All the characteristics of these resistors, however, such as their geometric dimensions and the exact makeup of the alloy they are made of, are covered by trade secret. Though we are unable to furnish an exact calculation of their contribution to the heat emitted by the rods, the short lengths of Inconel cable inside the rods allow us to reasonably consider it as lying within the error percentage associated to the measurements.

By adding the watts emitted directly by the dummy reactor to watts released by conduction to the rods, we get the dummy's thermal power output:

$$(316.50 \pm 4.11) + (129.86 \pm 6.49) = 446.36 \pm 10.60 = 446 \pm 2.4\% \text{ [W]} \quad (25)$$

Let us now compare this dissipated power with the power supply, the average of which over 23 hours of test is = (486 ± 24) W (uncertainty here is 5% of average, calculated as standard deviation). Keeping in mind the Joule heating of the power cables discussed in paragraph 4.3, we have the following results:

Power supply (W)	Joule heating (W)	Actual input (W)	Output (W)
486 ± 24	7	486 – 7 = 479 ± 24	446 ± 10

If we take error percentages into account, we will see that where input is at minimum possible value (455 W) and output at maximum possible value (456 W), our method overestimates by about 1 W, i.e. 0.2%. Vice versa, where input is at maximum possible value (503 W) and output at minimum possible value (436 W) our method underestimates the power supplied to the reactor by about 67 W, i.e. 14%.

We can therefore rely on the fact that applying the very same procedure to data gathered from the E-Cat test does not lead to any significant overestimation; rather, there is a good chance that the power actually generated by the reactor is underestimated.

6. Analysis of data obtained from the E-Cat

Using the same procedure employed for the dummy reactor, we analyzed the 16 files relevant to the active E-Cat test. For each file, we calculated average power emitted by radiation and convection by the reactor, cable dissipation through Joule heating, and power transmitted to the hollow rods. For the rods, we do not have 16 thermography files corresponding to those saved for the reactor, because, as mentioned above, the IR camera's position was changed frequently. We therefore analyzed several thermography files relevant to different days and positions, from which the two most representative ones for length of time and average temperatures were singled out. The first file refers to the days of the test before the 6th of March (the day in which power supply to the reactor was increased), the second to the following days. This choice was justified by the fact that the thermal variations on the rods obtained by analyzing the file data were significant only in the comparison between the two above-mentioned stages, and lay in any case within the percentage error associated to the result (± 5%). Once again, as in the case of the dummy reactor, the rods' symmetric geometry allowed us to perform calculations for only one set of three rods, and multiply the result by a factor of two. Here, from the power value obtained for the rods, one should once again subtract the small contribution of heat emitted by the cables that run through them; but this value is included in the percentage error associated to the result.

The results obtained are as follows:

	Radiation (W)	Convection (W)	Total for 1 set of three (W)	Total for 2 sets (W)
Rods, 1st period	72.15	81.84	153.99	307.98
Rods, 2nd period	88.47	87.94	176.41	352.82

Table 5. Power emitted by radiation and convection by a set of three E-Cat rods (column 4) and by both sets (column 5). The values are averaged over two different periods of time: the upper row refers to the days before March 6 – the day when the power supply was raised by ca. 100 watts – the lower row refers to the following days.

Tables 6 and 7 report all the E-Cat test results relevant to the days of testing, approximately two days for each file.

The first table shows the average temperature of each cap and of the entire body of the E-Cat for each of the 16 files analyzed. It should be mentioned that, as in the case of the dummy reactor, analysis on the E-Cat was again performed by dividing the thermal images into 10 areas along the length of the reactor, and into three

areas for each cap. In the table, however, the results relevant to each area are further averaged out, in order to facilitate reading.

In the second table, mean power consumption, watts produced and watts dissipated by Joule heating are shown for each file. Uncertainty associated to the result is on average 5% for power consumption and 3% for watts emitted. The last two columns record COP and net production. COP is the ratio of the sum of the mean power, emitted by radiation and convection by both the E-Cat and the rods, to mean power consumption of the reactor minus watts dissipated by the cables through Joule heating. It therefore gives an indicative parameter of the reactor's performance. Net production, on the other hand, is given by the difference between the total watts produced by the reactor and those consumed by it, and shows what portion of emitted power is entirely due the internal reaction of the E-Cat. By way of example, using the data of file No. 1 in the table, we have:

$$COP = (2128.32 + 307.98) / (815.86 - 37.77) = 3.13 \pm (3\% + 5\%) = 3.13 \pm 8\% \quad (26)$$

$$\text{Net Production} = (2128.32 + 307.98) - (815.86 - 37.77) =$$

$$= (2436.30 - 778.09) \pm (73.09 + 38.90) = 1658.21 \pm 111.99 = 1658 \pm 7\% \text{ [W]} \quad (27)$$

File No.	E-Cat body average T (°C)	Cap 1 average T (°C)	Cap 2 average T (°C)
1	1260.00	548.59	539.30
2	1257.77	550.71	541.93
3	1256.09	548.67	540.58
4	1257.21	549.02	539.22
5	1243.40	551.51	543.74
6	1398.99	609.24	589.93
7	1405.58	609.16	590.17
8	1404.04	607.84	589.06
9	1401.46	606.11	588.00
10	1392.26	600.51	601.34
11	1396.49	608.23	602.23
12	1400.86	610.10	604.65
13	1401.59	608.58	604.70
14	1400.56	607.45	604.62
15	1410.27	614.53	605.81
16	1412.31	611.09	595.15

Table 6. Average temperatures of E-Cat body and caps calculated for each of the 16 thermography files recorded during the test. One file corresponds to ca. two days of data logged.

File No.	Consumption (W)	Radiation (W)	Convection (W)	TOT. (W)	Rods (W)	Joule heating (W)	COP	Net Production (W)
1	815.86	1740.98	387.34	2128.32	307.98	37.77	3.13	1658.21
2	799.84	1733.30	386.46	2119.76	307.98	36.98	3.18	1664.88
3	791.48	1724.95	385.23	2110.18	307.98	36.49	3.20	1663.17
4	790.69	1729.30	385.49	2114.79	307.98	36.41	3.21	1668.49
5	785.79	1676.89	381.43	2058.32	307.98	36.13	3.16	1616.64
6	923.71	2381.64	427.64	2809.28	352.82	42.43	3.59	2280.82
7	921.91	2416.68	429.64	2846.32	352.82	42.18	3.64	2319.41
8	918.24	2407.26	429.16	2836.42	352.82	41.89	3.64	2312.89
9	917.90	2392.29	427.82	2820.11	352.82	41.75	3.62	2296.78
10	913.40	2348.43	425.64	2774.07	352.82	41.93	3.59	2255.42
11	904.77	2373.08	427.23	2800.31	352.82	41.52	3.65	2289.88
12	906.98	2397.95	428.56	2826.51	352.82	41.60	3.67	2313.95
13	910.47	2401.80	429.87	2831.67	352.82	41.62	3.67	2315.64
14	908.13	2394.93	428.70	2823.63	352.82	41.55	3.67	2309.87
15	905.01	2451.10	432.02	2883.12	352.82	41.46	3.75	2372.39
16	906.31	2454.71	431.47	2886.18	352.82	41.25	3.74	2373.94

Table 7. For each of the 16 thermography files recorded (ca. two days of test) we have, subsequently: average power consumption of the E-Cat, power emitted by the E-Cat by radiation, power emitted by convection, sum total of the last two values, sum total of watts emitted by both sets of rods by radiation and convection, power dissipated by Joule heating, COP, and net production.

What immediately stands out in Table 7 is the sharp difference between values obtained in the first ten days of the test (files 1 to 5 included), when power input to the reactor was kept at lower levels, and those obtained in the second period, in which power supply was increased by slightly more than 100 W. The effect of raising power input was an increase in power emission of about 700 W. Plot5 shows the trend of average temperature for one of the areas in which the thermography file of the E-Cat was divided (Area No. 5), when power input was increased. All values have been calculated by setting only one emissivity value, so as to make displaying on a continuous line possible, but the choice of ε is appropriate here only for the final temperatures reached after power increase. For this reason, the plot is not entirely reliable as far as the values on the *y*-axis are concerned: its purpose is merely that of showing how long it took the E-Cat to stabilize after input current was increased. As one can see, this amounts to about 400 seconds, slightly more than six minutes.

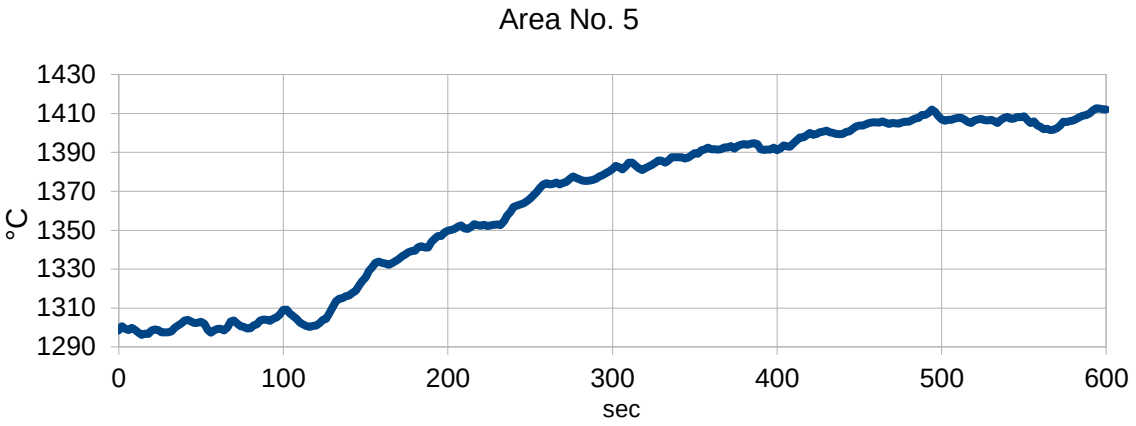

Plot 5. Average temperatures of Area 5 at the time of power supply increase. All values seen here are calculated assuming the same emissivity, in order to allow visualization on a continuous line. Thus, the *y*-axis is an arbitrary scale by which one can determine how long it took the E-Cat to reach a stable state (about 400 seconds) when input current was increased.

Another matter for consideration that stands out from the analysis of the results regards the trend of net production vs. that of consumption. There seems to be an anticorrelation between the two behaviors, which stands out as a decrease in average consumption values corresponding to increases in production averages, and vice versa. This behavior is probably due to a feedback effect driving the resistor power supply, raising it or lowering it according to the internal temperatures read by the thermocouple. The values of Table 7, relevant to net production, average consumption, and COP, are reproduced in Plots 6, 7, and 8.

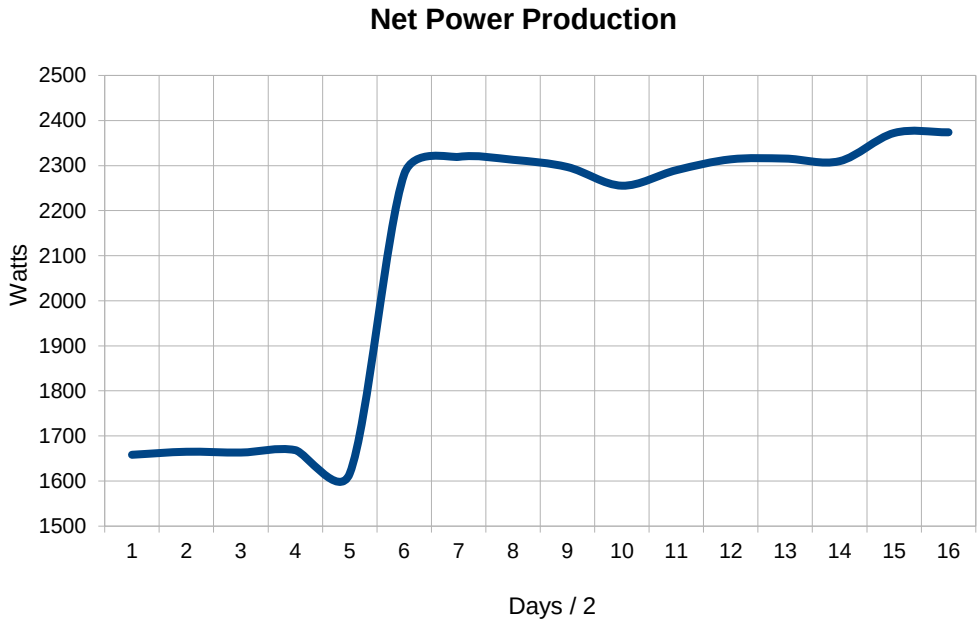

Plot 6. E-Cat Net power production trend throughout the test. Each interval on the *x*-axis represents a time span of about two days. Net power production is given by the difference between the total watts produced by the reactor and the watts consumed by it. It shows how much emitted power is exclusively due to the E-Cat's internal reaction.

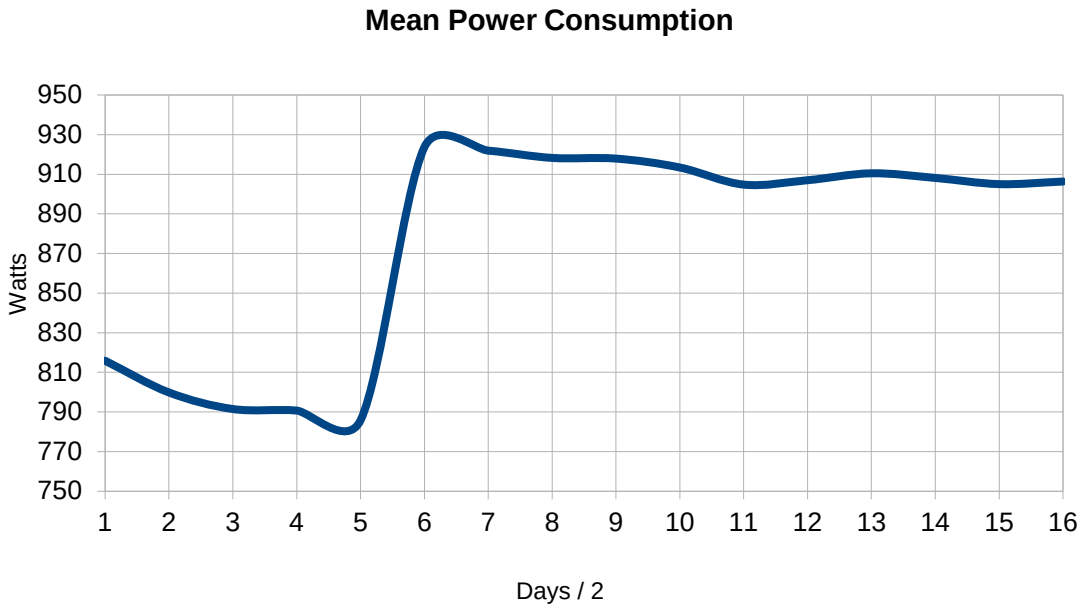

Plot 7. Mean power consumption of the E-Cat throughout the test. Each interval on the *x*-axis represents a time span of about two days.

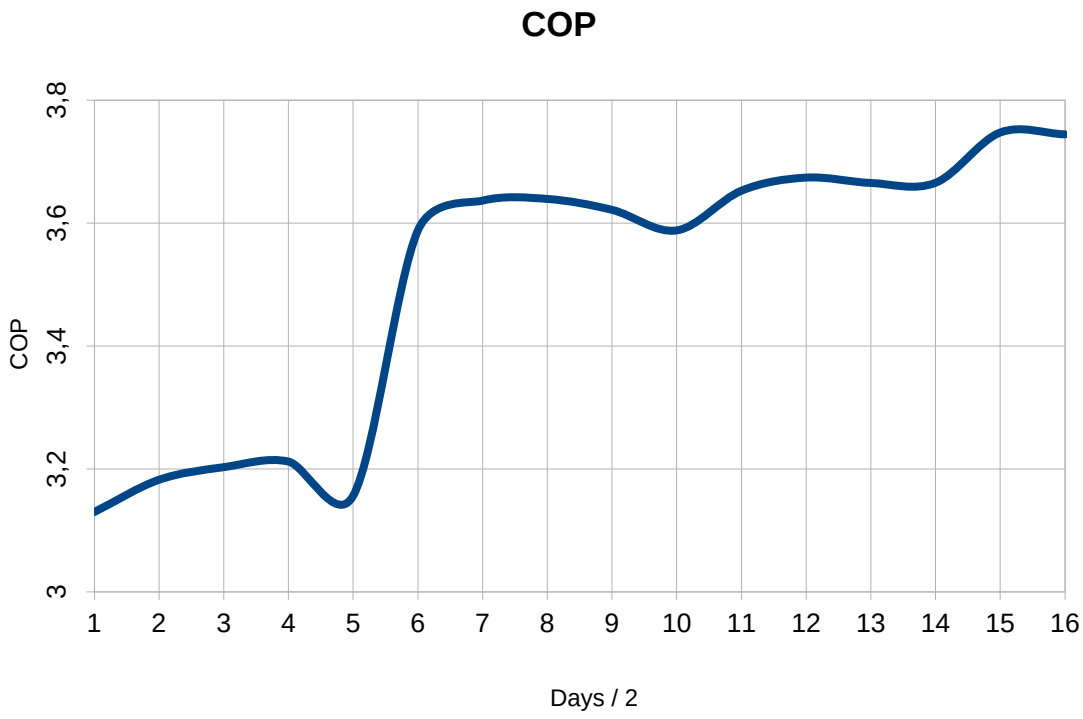

Plot 8. COP trend throughout the test. Each interval on the *x*-axis represents a time span of about two days. COP is the ratio of the sum of mean power emitted by radiation and convection by the E-Cat and by the rods, to the mean power consumption of the reactor minus power dissipated by Joule heating. It gives an indication of the E-Cat's performance.

It must be remarked that the COP values quoted here refer only to the performance of the reactor running at the capacity selected by us, not at its maximum potential, any evaluation of which lies beyond the purposes for which this test was designed. Awareness of the fact that the test would have lasted a considerable length of time prompted us to keep the reactor running at a level of operation capable of warranting both the stability and the safety of the test. Therefore, we do not know what the limits of the current technology are, in terms of performance and life span of the charges.

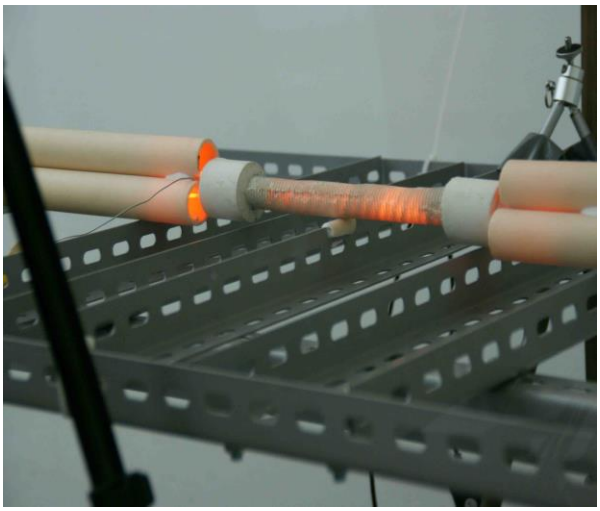

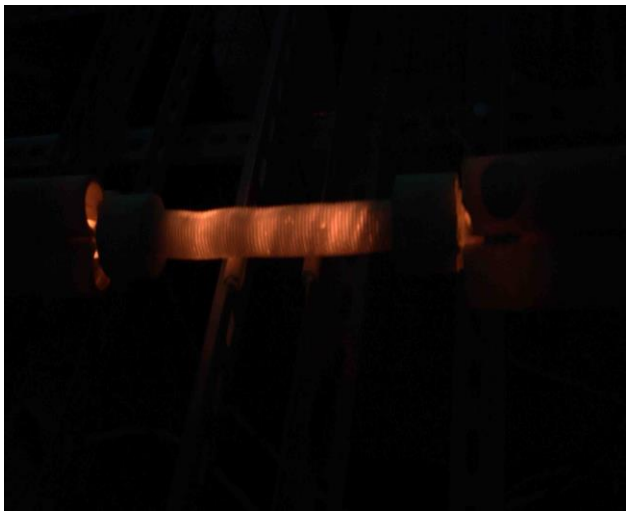

Figures 12a, 12b. E-Cat operating during the test. Note the Inconel resistors leaving the caps and entering the rods, where they are connected to the copper cables of the power supply. The resistors appear to glow intensely in the parts lying outside the caps, whereas inside the reactor body they seem to shade an underlying emission of light. This may be explained if we consider that the main source of energy inside the reactor body is actually the charge, and that it is emitting more light than the resistors. These are not visible through the caps, which are thicker than the reactor body. Upon leaving the reactor, however, the resistors emit heat almost exclusively by radiation (convection is negligible here, as they are inside the rods): there are no brighter sources of light which can "outshine" them, nor masses of alumina that can cool them. Their temperature is moreover fairly high, on account of the current they carry and the heat extracted by conduction from the reactor. Figure 12b was taken in the dark, from the opposite side to that of 12a. One of the three sets of hollow rods is visible, and another patch of insulating alumina cement on the second metal strut in the middle, added without modifying the setup.

7. Ragone Plot

The net production of the E-Cat, the values of which may be seen in the last column of table 7, allows us to calculate the total energy produced by the reactor during its ca. 768 hours of operation.

By multiplying the value of each file by the length of time that the file refers to (48 hours) and adding the results, we get:

$$(1658.21 \cdot 48) + (1664.88 \cdot 48) + \ldots + (2373.94 \cdot 48) = (1618194 \pm 10\%)\ [\text{Wh}] =$$

$$= (5825 \pm 10\%)\ [\text{MJ}] \qquad (28)$$

Next, we may calculate the specific gravimetric energy and the power density associated to the E-Cat and try to place it within the Ragone plot (Figure 13), a diagram comparing the power and energy densities of several conventional sources [11].

If one considers the weight of the charge = 1 g, one gets the following values relevant to thermal energy density and power density:

$$(1618194 / 0.001) = (1618194000 \pm 10\%)\ [\text{Wh/kg}] = (1.6 \cdot 10^9 \pm 10\%)\ [\text{Wh/kg}] =$$

$$= (5.8 \cdot 10^6 \pm 1\ 0\%)[\text{MJ/kg}] \qquad (29)$$

$$(1618194000 / 768) = (2107023 \pm 10\%)\ [\text{W/kg}] = (2.1 \cdot 10^6 \pm 10\%)\ [\text{W/kg}] \qquad (30)$$

These results place the E-Cat beyond any conventional source of energy, as may be clearly seen from the plot in Figure13. Our values, though close to the energy densities of nuclear sources, such as U235, are however lower than the latter by at least one order of magnitude [12].

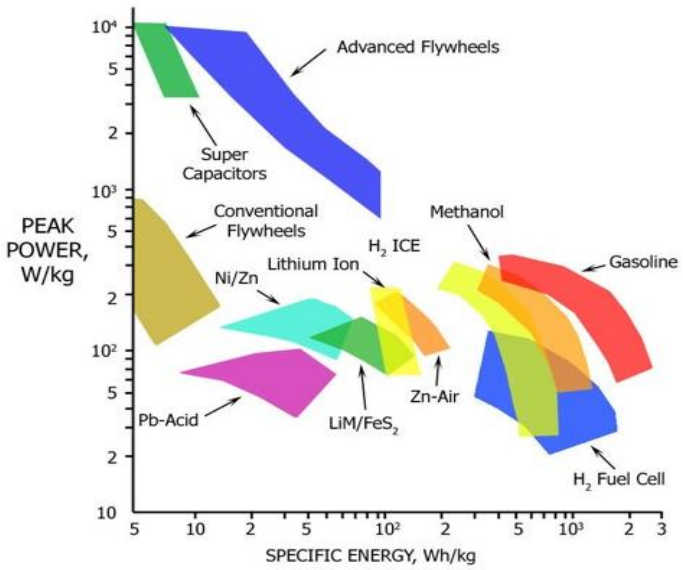

Figure 13. "Ragone plot of energy storage"[11]. The plot shows specific gravimetric energy and power densities relevant to various sources. The E-Cat, which would be far off the scale here, lies outside the region occupied by conventional sources.

Considering that we do not know the internal structure of the reactor, and therefore cannot completely rule out that there were other charges inside it besides the one weighed and inserted by us, we may repeat the above calculations taking the weight of the entire reactor (452 ± 1 g) into consideration:

$(1618194 / 0.452) = (3580075 \pm 10\%)$ [Wh/kg] $= (3.6 \cdot 10^6 \pm 10\%)$ [Wh/kg] =

$= (1.3 \cdot 10^4 \pm 10\%)$ [MJ/kg] (31)

$(3580075 / 768) = (4661 \pm 10\%)$ [W/kg] $= (4.7 \cdot 10^3 \pm 10\%)$ [W/kg] (32)

Even if taken from this extremely conservative point of view, the reactor lies beyond the limits of the above Ragone plot.

Lastly, by way of further enquiry, we may consider another kind of Ragone plot, where volumetric densities instead of gravimetric densities are expressed (Figure 14), and calculate the reactor's position with respects to it [13].

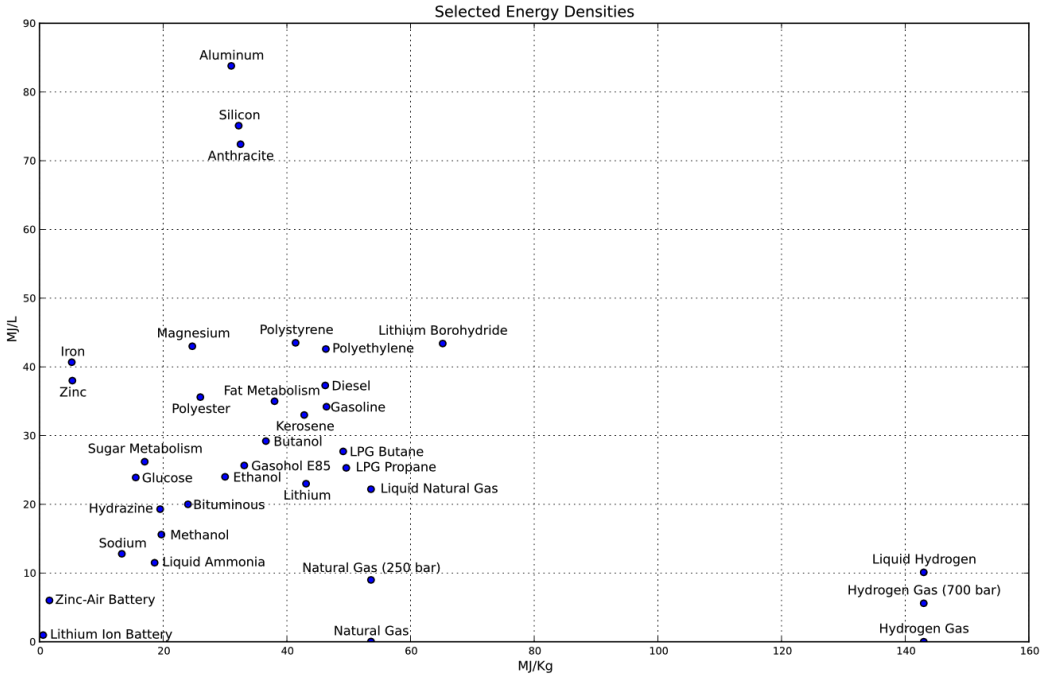

Figure 14. Another version of the Ragone Plot of Energy Storage [13]. In this plot, specific volumetric and gravimetric energy densities are given for various sources. The E-Cat, far off the scale here, lies outside the region occupied by conventional chemical sources.

Given that we do not know the exact internal volume of the E-Cat, we may conservatively take into account the whole external volume of the object. The results are:

$$\text{E-Cat Volume} = 20\pi + 2 \cdot 16\pi = (163 \pm 2\%)\ \text{cm}^3 = (0.163 \pm 2\%)\ \text{l} \qquad (33)$$

$$(5825 / 0.163) = (35736 \pm 12\%)\ [\text{MJ/l}] = (3.6 \cdot 10^4 \pm 12\%)\ [\text{MJ/l}] \qquad (34)$$

Once again, even in the most conservative scenarios, we have values that allow us to conclude that the reactor studied here may not be considered a conventional source of energy.

8. Fuel analysis

The result from the heat measurement is remarkable by giving such a large amount of heat from the very small quantity of fuel powder used confined in the small volume of the reactor. This large amount of heat is, as pointed out above, way beyond what can be expected from chemical burning, which only involves rearrangements of the fuel material at the atomic scale, i.e. by transforming atomic binding energies to kinetic energy. Very large energy transformations can only take place when binding energies at the nuclear level are exploited, as in fusion reactions for light elements and fission reactions for heavy elements. However fusion reactions between free charged particles are extremely unlikely at low energies due to the Coulomb barrier. The conditions for fusion reactions between particles imbedded in a specific metal compound are not expected to be very much different from those of free particles, but this is not known in all details. It is therefore not possible to categorically reject the occurrence of fusion reactions in a metal compound having specific properties, by referring to our knowledge of the fusion process between free particles. In fact, as an example, the d(d,p)t fusion reaction cross sections have been observed [14] to depend on the temperature in deuterated metals at sub-Coulomb energies. This is an effect of screening from the electron cloud surrounding the interacting nuclei. In Astrophysics it is also well known that low energy cross sections are higher than expected [see e.g. 14,15].Whether fusion reactions can be induced at a large scale in a metal compound under specific conditions is an open question.

In order to get information on wheter any rearrangement at the nuclear level takes place in the fuel during the burning process in the E-Cat, we studied the isotopic composition of the fuel before and after the burning. Any change in the isotopic composition of the fuel in E-Cat is expected to have its origin in a nuclear reaction. The element analyses were performed by three different external groups, each specialized in the different techniques employed. The work begun with an electron microscopy (SEM) scan to study the surface morphology of the fuel powder. The analyzing methods employed were X-ray Photoelectron Spectroscopy (XPS), Dispersive X-ray Spectroscopy (EDS), Secondary Ion Mass Spectrometry (SIMS) and chemical analysis from Inductively Coupled Plasma Mass Spectrometry (ICP-MS) as well as atomic emission spectroscopy (ICP-AES). The full report from these analyses is presented in detail in the Appendices 3 and 4.

The XPS gives information on which elements are present in the fuel, while the SIMS and ICP-MS analyzing methods also give the isotopic composition of the nuclear species. The ICP-AES analysis also gives the masses percentage of the found elements. Both XPS and SIMS give information on which elements are present at the surface of a sample granule down to a depth of a few nanometers. The ICP-MS is an integrating method giving the average isotopic composition of the whole fuel/ash sample being analyzed. The ICP-AES also gives the mass values in the whole sample. It is thus quite plausible that the four methods give rather different results depending on the sample granule chosen as well as in the case where the whole sample is used, provided that the burning process in the fuel is not even but varies locally as observed. However, qualitatively the methods should yield the same results. It should also be noted that our total sample was about 10 mg, i.e. only a small part of the total fuel weight of 1 g used in the reactor. The sample was taken by us at random from the fuel and ash, observing utmost care to avoid any contamination.

An arbitrary sample of different granules is chosen for the analysis, but the same samples are used for both EDS and SIMS. The fuel contains natural nickel powder with a grain size of a few microns. The existence of natural Nickel content is confirmed by all four analyzing methods being used. In addition the fuel is found to be mixed with a component containing hydrogen, i.e. probably a chemical hydride. From all combined analysis methods of the fuel we find that there are significant quantities of Li, Al, Fe and H in addition to Ni. Moreover from the EDS and XPS analysis one finds large amounts of C and O. It should be stressed, that the quantities of most elements differ substantially depending on which granule is analyzed. In addition to these elements there are small quantities of several other elements, but these can probably be considered as impurities.

It is plausible that the fuel is mixed with the standard Lithium Aluminum Hydride, $LiAlH_4$. Further evidence of that is obtained from the ICP-AES analysis which shows that the mass ratio between Li and Al is compatible with a $LiAlH_4$ molecule. This compound can be used to produce free hydrogen by heating. We remark in particular that hydrogen but no deuterium was seen by SIMS. The other methods are insensitive to both hydrogen and deuterium.

The ash has a different texture than the powder-like fuel by having grains of different sizes, probably developed from the heat. The grains differ in element composition, and we would certainly have liked to analyze several more grains with SIMS, but the limited amount of ash being available to us didn't make that possible. The main result from our sample is nevertheless clear, that the isotopic composition deviates dramatically from the natural composition for both Li and Ni.

The Lithium content in the fuel is found to have the natural composition, i.e. ^{6}Li 7 % and ^{7}Li 93 %. However at the end of the run a depletion of ^{7}Li in the ash was revealed by both the SIMS and the ICP-MS methods. In the SIMS analysis the ^{7}Li content was only 7.9% and in the ICP-MS analysis it was 42.5 %. This result is remarkable since it shows that the burning process in E-Cat indeed changes the fuel at the nuclear level, i.e. nuclear reactions have taken place. It is notable, but maybe only a coincidence, that also in Astrophysics a ^{7}Li depletion is observed [see e.g. 17].

One can speculate about the nature of such reactions. Considering Li and disregarding for a moment from the problem with the Coulomb barrier the depletion of ^{7}Li might be due to the reaction $p + {}^{7}Li \rightarrow {}^{8}Be \rightarrow {}^{4}He + {}^{4}He$. The momentum mismatch in the first step before ^{8}Be decays can be picked up by any other particle in the vicinity. In this case the large kinetic energy of the ^{4}He (distributed between 7 and 10 MeV) is transferred to heat in the reactor via multiple Coulomb scattering in the usual stopping process. One can then estimate how much this reaction contributes to the total heat being produced in our test run. From the ICP-AES analysis we find that there is about 0.011 gram of ^{7}Li in the 1 gram fuel. If each ^{7}Li nucleus releases about 17 MeV we find then that the total energy available becomes 0.72 MWh. This is less than the 1.5 MWh actually produced in our 32 days run, so more energy has to come from other reactions, judging from this very rough and speculative estimate.

Another remarkable change in the ash as compared to the unused fuel is the identified change in the isotope composition of Ni. The unused fuel shows the natural isotope composition from both SIMS and ICP-MS, i.e. ^{58}Ni (68.1%), ^{60}Ni (26.2%), ^{61}Ni (1.1%), ^{62}Ni (3.6%), and ^{64}Ni (0.9%), whereas the ash composition from SIMS is: ^{58}Ni (0.8.%), ^{60}Ni (0.5%), ^{61}Ni (0%), ^{62}Ni (98.7%), ^{64}Ni (0%), and from ICP-MS: ^{58}Ni (0.8%), ^{60}Ni (0.3%), ^{61}Ni (0%), ^{62}Ni (99.3%), ^{64}Ni (0%). We note that the SIMS and ICP-MS give the same values within the estimated 3% error in the given percentages.

Evidently, there is also an isotope shift in Nickel. There is a depletion of the ^{58}Ni and ^{60}Ni isotopes and a buildup of the ^{62}Ni isotopes in the burning process. We note that ^{62}Ni is the nucleus with the largest binding energy per nucleon. The origin of this shift cannot be understood from single nuclear reactions involving protons. With alpha particles colliding with Ni one can in principle raise the atomic mass number by 4 via exciting ^{58}Ni to ^{62}Zn, which then via positron emission decays back to ^{62}Cu and ^{62}Ni, but that is hardly believable to occur due to an enormous Coulomb barrier to merge ^{4}He and Ni. Besides, with this reaction one can also go to stable Zn isotopes, which are not found in the ash.

It should be pointed out that the fusion towards heavier isotopes of Nickel releases energy. For example the reaction $p + {}^{58}Ni \rightarrow {}^{59}Cu + \gamma$ and ^{59}Cu decaying back to ^{59}Ni via β^{+} emission releases 3.4 MeV. Even if that particular reaction is excluded, since no gammas are observed, we can tentatively use this number for each step towards ^{62}Ni, and the information from ICP-AES that there is about 0.55 gram Ni in the fuel. We find then that there is about 2.2MWh available from the Nickel transformations. Accordingly, from Nickel and Lithium together there is about 3 MWh available, which is twice the amount given away in the test run. Consequently we can conclude that the amount of fuel is probably compatible with the energy release being measured, although a quantitative statement requires detailed knowledge of the prevailing reactions.

However, as discussed above, it is of course very hard to comprehend how these fusion processes can take place in the fuel compound at low energies. Presently we should therefore restrict ourselves to merely state that an isotope shift has occurred in Lithium and Nickel. We refrain from speculations in any dynamic scenario making this reaction possible at low energies. The reaction speculation above should only be considered as an example of reasoning and not a serious conjecture.

If nuclear transitions are prevalent in the burning process it is expected that radiation is emitted. It is remarkable that neither neutrons, charged particles nor gammas are observed from the E-cat reactor. Furthermore, the spent fuel was found inactive right after the E-Cat run was stopped. All imaginable nuclear reactions in the reactor should be followed by some radiation, and at least some of that radiation should penetrate the reactor wall and be possible to detect. Even in the case discussed above with two rather high energy helium nuclei in the final state, which all stop in the reactor, one can expect that some helium nuclei during the stopping process undergo some nuclear reaction, e.g. inelastic scattering of ^{4}He on Li, Al or Ni which then subsequently decays to their ground state respectively via gamma emission. To get free neutron is however not kinematically possible with the 10 MeV alpha available. The absence of any nuclear radiation from the burning process is presently an open question, and has to be understood.

9. Summary and concluding remarks

A 32-day test was performed on a reactor termed E-Cat, capable of producing heat by exploiting an unknown reaction primed by heating and some electro-magnetic stimulation. In the past years, the same collaboration has performed similar measurements on reactors operating in like manner, but differing both in shape and construction materials from the one studied here. Those tests have indicated an anomalous production of heat, which prompted us to attempt a new, longer test. The purpose of this longer measurement was to verify whether the production of heat is reproducible in a new improved test set-up, and can go on for a significant amount of time. In order to assure that the reactor would operate for a prolonged length of time, we chose to supply power to the E-Cat in such a way as to keep it working in a stable and controlled manner. For this reason, the performances obtained do not reflect the maximum potential of the reactor, which was not an object of study here.

Our measurement, based on calculating the power emitted by the reactor through radiation and convection, gave the following results: the net production of the reactor after 32 days' operation was (5825 ± 10%) [MJ], the density of thermal energy (if referred to an internal charge weighing 1 g) was ($5.8 \cdot 10^6$ ± 10%) [MJ/kg], while the density of power was equal to ($2.1 \cdot 10^6$ ± 10%) [W/kg]. These values place the E-Cat beyond any other known conventional source of energy. Even if one conservatively repeats the same calculations with reference to the weight of the whole reactor rather than that of its internal charge, one gets results confirming the non-conventional nature of the form of energy generated by the E-Cat, namely ($1.3 \cdot 10^4$ ± 10%) [MJ/kg] for thermal energy density, and ($4.7 \cdot 10^3$ ± 10%) [W/kg] for power density.

The quantity of heat emitted constantly by the reactor and the length of time during which the reactor was operating rule out, beyond any reasonable doubt, a chemical reaction as underlying its operation. This is emphasized by the fact that we stand considerably more than two order of magnitudes from the region of the Ragone plot occupied by conventional energy sources.

The fuel generating the excessive heat was analyzed with several methods before and after the experimental run. It was found that the Lithium and Nickel content in the fuel had the natural isotopic composition before the run, but after the 32 days run the isotopic composition has changed dramatically both for Lithium and Nickel. Such a change can only take place via nuclear reactions. It is thus clear that nuclear reactions have taken place in the burning process. This is also what can be suspected from the excessive heat being generated in the process.

Although we have good knowledge of the composition of the fuel we presently lack detailed information on the internal components of the reactor, and of the methods by which the reaction is primed. Since we are presently not in possession of this information, we think that any attempt to explain the E-Cat heating process would be too much hampered by the lack of this information, and thus we refrain from such discussions.

In summary, the performance of the E-Cat reactor is remarkable. We have a device giving heat energy compatible with nuclear transformations, but it operates at low energy and gives neither nuclear radioactive waste nor emits radiation. From basic general knowledge in nuclear physics this should not be possible. Nevertheless we have to relate to the fact that the experimental results from our test show heat production beyond chemical burning, and that the E-Cat fuel undergoes nuclear transformations. It is certainly most unsatisfying that these results so far have no convincing theoretical explanation, but the experimental results cannot be dismissed or ignored just because of lack of theoretical understanding. Moreover, the E-Cat results are too conspicuous not to be followed up in detail. In addition, if proven sustainable in further tests the E-Cat invention has a large potential to become an important energy source. Further investigations are required to guide the interpretational work, and one needs in particular as a first step detailed knowledge of all parameters affecting the E-Cat operation. Our work will continue in that direction.

Acknowledgments

By this work the authors would like to deeply and at heart honor the late Sven Kullander, who initiated this independent test experiment. He was a great source of inspiration and knowledge throughout the course of this work.

The authors gratefully acknowledge Andrea Rossi and Industrial Heat LLC for providing us with the E-cat reactor to perform an independent test measurement. The authors would like to thank Prof. Ennio Bonetti (University of Bologna) and Prof. Alessandro Passi (University of Bologna [ret.]) for critical reading of the manuscript.

All authors of the appendices are gratefully acknowledged for their valuable contribution to this work.

This paper was partially sponsored by the Royal Swedish Academy of Sciences, and Elforsk AB.

We would also like to thank Officine Ghidoni SA for putting their laboratory at our disposal and allowing use of their AC power.

Lastly, our thanks to Industrial Heat LLC (USA) for providing financial support for the measurements performed for radiation protection purposes.

References

[1] G. Levi et al, *Indication of anomalous heat energy production in a reactor device containing hydrogen loaded nickel powder,* http://arxiv.org/abs/1305.3913.

[2] Optris, *Basic principles of non-contact temperature measurement*, www.optris.com.

[3] R. Morrell, *Handbook of properties of technical and engineering ceramics Part 2*, 1985, H.M.S.O.

[4] A. Gillespie, S. Rokugawa, *A temperature and emissivity separation algorithm for advanced spacebornethermal emission and reflection radiometer (ASTER) images*, IEEE Transactions on Geoscience and Remote Sensing, VOL. 36, N. 4, July 1998.

[5] Volker Tank, *Method for the contactless radiation measurement of the temperature of an object independent of its emissivity, and device for carrying out this method*, EP0129150.

[6] J.M. Coulson and J.F. Richardson, *Chemical Engineering*, 1999 (sixth edition), Butterworth Heinemann.

[7] E. Hahne, D. Zhu, *Natural convection heat transfer on finned tubes in air*, Int. J. Heat Mass Transfer, Vol. 37 (59-63), 1994 Elsevier Science Ltd.

[8]A.D. Kraus, A. Aziz, *Extended surface heat transfer*, 2001, John Wiley & Sons Inc.

[9] T.L. Bergman, A.S. Lavine, *Fundamentals of heat and mass transfer*, 2011 (seventh edition), John Wiley & Sons Inc.

[10] A. Bejan, A.D. Kraus, *Heat Transfer Handbook*, 2003, John Wiley & Sons Inc.

[11] A. F. Ghoniem, *Needs, resources and climate change: clean and efficient conversion technologies*, Progress in Energy and Combustion Science 37 (2011), 15-51, fig.38.

[12] http://www.whatisnuclear.com/physics/energy_density_of_nuclear.html.

[13]http://en.wikipedia.org/wiki/File:Energy_density.svg.

[14] R. Raiola et al. *Enhanced d(d,p)t fusion reaction in metals,* Eur. Phys. J. A 27, s01, 79-82 (2006)

[15] LUNA Collaboration, J. Cruz et al, *Electron screening in ^{7}Li(p, α)α and ^{6}Li(p, α) 3He for different environments*, Physics Letters B 624 (2005) 181–185.

[16] C.Rolf , *Nuclear reactions in stars far below the Coulomb barrier*, Progress in Particle and Nuclear Physics 59 (2007) 43–50.

[17] n_TOF Collaboration, M.Barbagallo et al. *Measurement of ^{7}Be(n,α)^{4}He and ^{7}Be(n,p)^{7}Li cross sections for the Cosmological Lithium Problem,*CERN-INTC-2014-049 / INTC-P-417, 05/06/2014.

Appendix 1

Radiation measurements during the long-term test of the E-Cat prototype.

D. Bianchini, Bologna

PREFACE

Between the 24/02/14 and the 29/03/14 in Lugano (CH) I performed the radiation field measurements for radiation protection purposes as per Andrea Rossi request on the 30/01/14.

As in previous evaluation on the same type of prototype, the process, the geometry and the materials are unknown. The industrial plant manager declared the absence of using both of charge particle acceleration systems and intentionally added radioisotopes of any type. This statement excludes the presence of a field of ionizing radiation except for a new and unknown form of radiation source .The radiation measurements are made on the materials used before and after the test and on the ambient around the prototype in use during the test. The measuring positions are conservative with respect to the position and the occupation time of the operators involved.

The present evaluation based on the radiation measurements cannot be related to criteria of functionality of the system and cannot be used for comparison in systems different from this one, in the process, in the geometry or in the construction materials used.

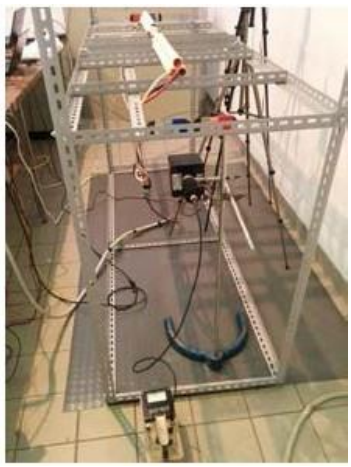

Figl: Picture of the neutron probe and tennoluminescent detectors around the prototype

MATERIALS AND METHODS

In order to avoid potential source or risk for the operators and the population around the prototype during the long duration test the commissioner ask me to measure different kind of radiation in wide range of energy. The hypothesis that the prototype can produce a radiation field is due to the unconventional energy that the inventor has produced with it. To ensure that this process do not involve ionizing radiation I perform the evaluations on different type of radiation in wide spectrum and wide energy. The measurements are divided temporally in before, during and after the using of the prototype. In the "before" and "after" evaluation the gamma and alpha/beta field evaluation are made on the material used inside the prototype. In the "during" evaluations the gamma and neutron field are performed around the system.

The measure does not take into account in any way the interaction of the photons, charged particles or neutron produced by the materials inside the apparatus during the using and cannot in any way be traced back to the production of ionizing radiation from the inside of the prototype.
The radiation measurement protocol is structured as follows:

- The comparison of the CPM collected during the test with the CPM referred to the background in laboratory is an index of low flounce radiation field.

- The active probes and the TLD positions was chosen to be at the closest position.
- accessible by operators around the support frame.

- The radioisotope presence in the material used before and after the experiment is
- evaluated with a Geiger scanner in ratemeter mode.

- The background radiation, for all kind of radiation, has been measured both in the plant and in laboratory, at a distances d>30m from the room where the test took place.

The measurements were performed with the following instrumentation:

1. LUDLUM 2241 Scaler-Ratemeter (sin 214522):

- Scintillation probe (2.5 x 2.5 cm) (Dia x L) (Nal)TI Ludlum 44-2 (PR-227268);
- Energy range: 50 keV -2 MeV;
- Exposure sensitivity: 19.9 CPM/nSv/hr ^{137}'Cs gamma);
- Integration time: 2s.
- Rate meter Alarm and Alert: 0.2 µSv/h
- Calibration factors on ^{137}Cs supplied by the factory (04/2012)
- Constancy evaluation of gamma response factor with ^{137}Cs radiation source before and after the test
- The rate meter has a serial RS-232 blue-tooth connection to a pc logger.

2. LUDLUM 2221 Sealer/Ratemeter SCA (sin202347):

- Neutron Radiation Detector (neutron recoil scintillator) Prescila 42-4 l (PR256816)
- Sensitivity declared : 350 cpm per mrem/h;
- Calibrations at ENEA calibration service:
  14/06/2012 (N°03N12) wi1h AmBe source (E.,.-, =4.4 MeV)
  F =0.028µS'vl h/ CPM I equivalent to 36 cpm per µSv/h
  28/0112008 wi1h Pu-Li source ($E_{neutrons}$ =0.54 MeV)
  F =0.067µS'vl h/ CPM equivalent to 15 cpm per µSv/h
- Angular dependence and temperature dependence as in Figure 2

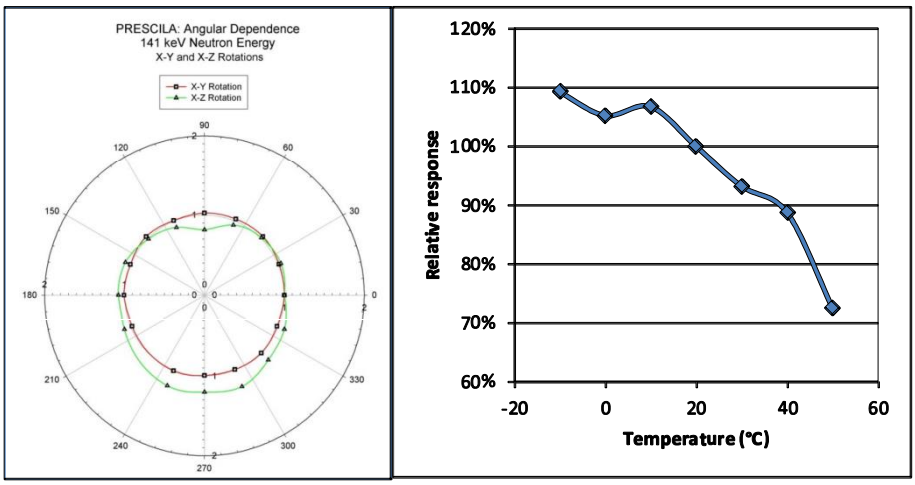

Figure 2: Angular and energy dependence of the Ludlum 44-41 neutron probe.

3. LUDLUM 2241 Sealer-Ratemeter (sin214522):

- Geiger Probe Ludlum 44-9 (PR- 226527);
- Energy range: energy dependent
- Exposure sensitivity: 3300 cpm/mR/hr (^{137}Cs gamma);
- Integration time: 2s.
- Background (typical): 60CPM
- Rate meter Alarm aod Alert: 0.3 μSv/h
- Calibration factors on ^{137}Cs supplied by the factory (0412012)
- Constancy evaluation of gamma response factor with ^{137}Cs before and after the test.

4. TERMOLUMINESCENT DOSIMETERS LiF:V

- TDL Reader: Vinteen Toledo 654
- Calibration field: IEC 61267 – Code RQR5 – 2.45 mm A1 HVL
- Calibration dose :0.050±0.005 mGy
- Calibration factor: individual for each TDL
  Mean counts of the sample: 1613 cou
  Mean F value of the sample 0.031 μC
- Extended error on the dose measure at 0.050n
- 2 TDL for each position of measurement
- Calibration made before and after the measurement

RESULTS

Evaluation of radionuclides presence:

The material that compound the prototype, include the material inside, are controlled before and after the test in order to avoid the presence of radioisotope contamination. These measurements are performed with the Geiger probe in rate meter configuration on at least 20 points:

	CPM (mean values)	
	BEFORE	AFTER
Backsuound radiation in laboratory	5l (σ =ll)	53 (σ =IO)
Background radiation in plant	47 (σ = 13)	48 (σ=13)
Naked "Hot-Cat"	53 (σ = 11)	51 σr = 12)
Sample of inside reactor material	55 (σ = 14)	52 (σ= 15)

The reactor's inside material has been scanned in a low background container (5cmPB) with the Nal probe and this measure didn't shows any γ/X activity of the sample.

Gamma/X monitoring during the test:

The monitoring of the photonic dose field is made with passive and active dosimeters. During the 34 days of running 16 TLD dosimeters recorded the dose (4 for each side) and 4TLD are used as control placed at d > 50cm (Figure 3).

Appendix 1

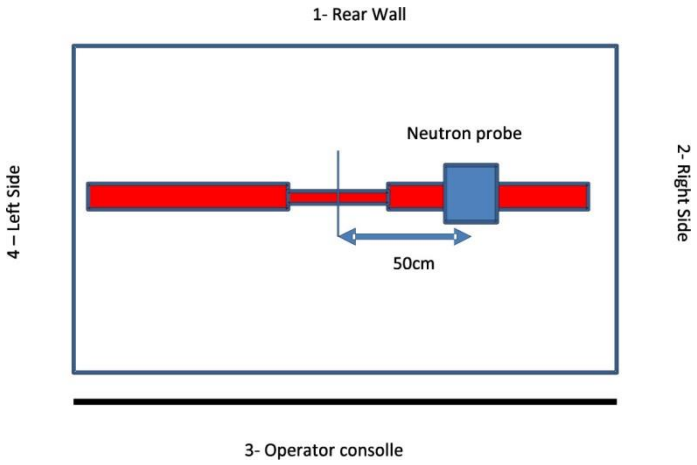

Figure 3. Relative position of the detector with respect to the prototype

The term luminescent reading values and relative doses are presented in table:

Position	***Counts***	***Dose (mGvl***
1 -Rear wall	2539	0.079±0.024
2 -Right side	2477	0.077±0.023
3 -Operator consolle	2411	0.075±0.022
4 -Left side	2553	0.079±0.024
Control	2385	0.074±0.022

The comparison of the absolute dose to the control dosimeters (background) shows that the increment dose due the test is less than 0.03±0.0lmGy for all the positions considered.

Neutron field monitoring during the test:

The neutron dose field evaluation is made on 5 hours interval. This interval is considered representative of the rest of the test. The measurements are performed in scaler mode on 60s integration time on the detailed number of runs.

	Number of runs	Mean Counts	Standard deviation
Background radiation in the laboratory	20	14.1	$\sigma = 4.3$
Background radiation in plant	45	13.8	$\sigma = 3.9$
50cm from the center of the prototype	95	16.9	$\sigma = 4.1$

Bologna 09/04/2014

Dott. Bianchini David
Via EmiliaPonente 37S
40132 -Bologna
P.l:01037800578

Appendix 2

Alumina sample analysis

Ennio Bonetti,
Department of Physics and Astronomy
University of Bologna.

In order to determine the nature of the material covering the reactor, a sample from one of the ridges was analyzed. To prevent contamination, the fragments were placed on an X-Ray crystallography slide and attached with high vacuum grease, avoiding further handling.

Figure shows slide with fragments attached.

A table of the measurements parameters used follows.

Anchor Scan Parameters:

Scan Axis	Gonio	Start Position [°2Th.]	30.0000
End Position [°2Th.]	100.0000	Step Size [°2Th.]	0.0200
Scan Step Time [s]	4.0000	Scan Type	Continuous
Offset [°2Th.]	0.0000	Divergence Slit Type	Fixed
Divergence Slit Size [°]	1.0000	Specimen Length [mm]	10,00
Receiving Slit Size [mm]	0.1000	Measurement Temperature [°C]	25.00
Anode Material	Cu	K-Alpha1 [Å]	1.54060
K-Alpha2 [Å]	1.54443	K-Beta [Å]	1.39225
K-A2 / K-A1 Ratio	0.50000	Generator Settings	45 mA, 45 kV
Diffractometer Type	Rigaku DMAX-IIIC	Diffractometer Number	1
Goniometer Radius [mm]	240.00	Dist. Focus-Diverg. Slit [mm]	91.00
Incident Beam Monochromator	No	Spinning	No

Appendix 2

Graphics: (Bookmark 2)

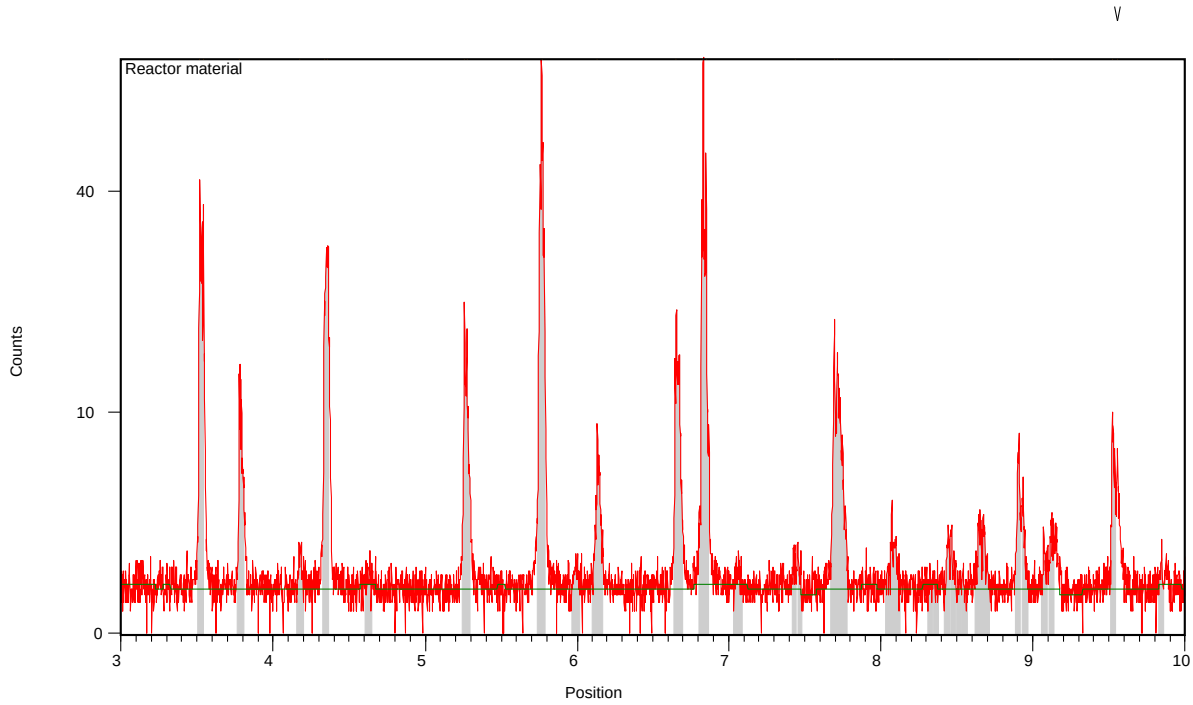

Analysis software automatically identified the following peak list from its database:

Peak List:

Pos. [°2Th.]	Height [cts]	FWHM [°2Th.]	d-spacing [Å]	Rel. Int. [%]	Tip width [°2Th.]	Matched by
35.1845	338.49	0.0787	2.55074	47.87	0.0945	00-042-1468; 01-071-1127
35.4333	331.09	0.0590	2.53340	46.83	0.0708	01-071-1127
37.7784	134.95	0.0590	2.38136	19.09	0.0708	00-042-1468
41.7685	9.88	0.2362	2.16263	1.40	0.2834	00-042-1468; 01-071-1127
43.3784	220.16	0.0960	2.08430	31.14	0.1152	00-042-1468
43.5753	280.81	0.2362	2.07706	39.72	0.2834	01-071-1127
52.5804	221.39	0.0960	1.73915	31.31	0.1152	00-042-1468
52.7386	185.66	0.0720	1.73862	26.26	0.0864	
57.6591	634.55	0.1200	1.59745	89.74	0.1440	01-071-1127
61.3068	71.69	0.1440	1.51086	10.14	0.1728	00-042-1468; 01-071-1127
66.5421	186.63	0.1920	1.40412	26.40	0.2304	00-042-1468
68.3309	707.06	0.0720	1.37165	100.00	0.0864	00-042-1468
68.5276	456.75	0.0720	1.37160	64.60	0.0864	
74.3991	5.84	0.5760	1.27408	0.83	0.6912	00-042-1468
76.9444	185.35	0.0960	1.23816	26.21	0.1152	00-042-1468
77.1776	144.63	0.1920	1.23500	20.46	0.2304	00-042-1468; 01-071-1127
80.8221	12.13	0.3840	1.18825	1.72	0.4608	00-042-1468; 01-071-1127
84.4963	10.90	0.3840	1.14570	1.54	0.4608	00-042-1468
86.4385	18.75	0.4800	1.12487	2.65	0.5760	00-042-1468
89.0923	77.91	0.1680	1.09810	11.02	0.2016	00-042-1468
91.2842	17.82	0.6720	1.07736	2.52	0.8064	00-042-1468
95.2206	96.29	0.1200	1.04295	13.62	0.1440	00-042-1468
95.5698	57.60	0.1440	1.04006	8.15	0.1728	

Peak configuration allowed the identification of the following components:

Appendix 2

Identified Patterns List:

Visible	Ref. Code	Score	Compound Name	Displacement [°2Th.]	Scale Factor	Chemical Formula
*	00-042-1468	75	Alumina	0,000	0,357	Al2 O3
*	01-071-1127	54	Corundum	0,000	0,211	Al2 O3

Plot of Identified Phases.

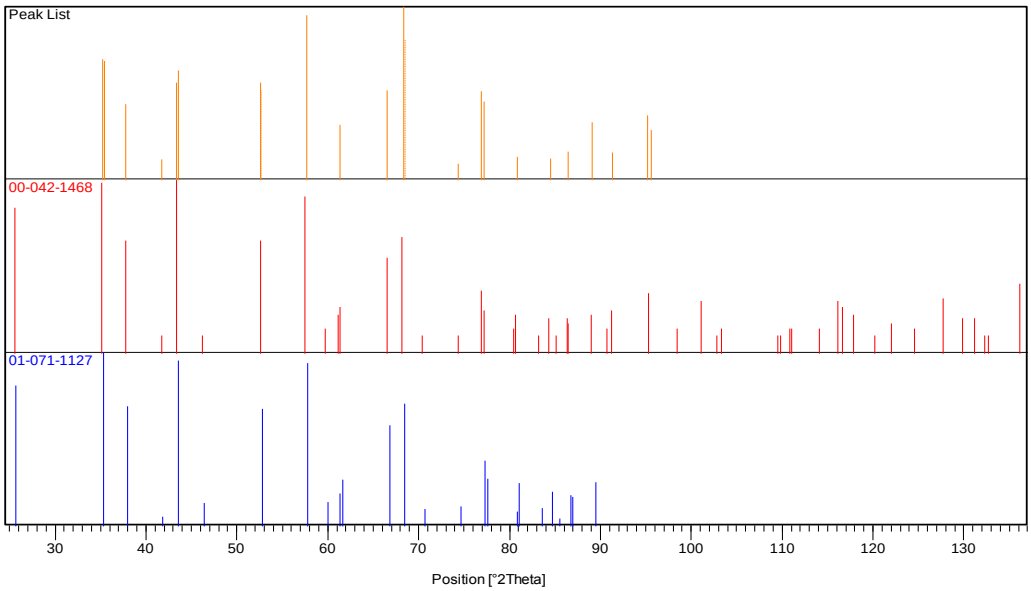

Figure shows peaks found (blue) compared to the two materials identified through the database (red).

Conclusion: within the limits of the instrument's sensitivity range, the sample appears to be constituted of aluminum dioxide, Al_2O_3.

Appendix 3

Investigation of a fuel and its reaction product using SEM/EDS and ToF-SIMS

Ulf Bexell and Josefin Hall

Materialvetenskap, Högskolan Dalarna

Background

Powder samples were investigated before and after an experiment performed in Lugano, Switzerland. The purpose of the present investigation is to study which elements that mainly occur in the samples.

Experimental

Material

Two types of powder samples were investigated. The first sample, called fuel, is declared to mainly contain Ni and probably some additions of H and Li. The second sample, called ash, is the reaction product of the fuel powder from an experiment performed in Lugano. The powder samples were mounted on a carbon adhesive sticker before analysis. The samples analyzed with SEM/EDS and ToF-SIMS were received mounted and analyzed as-received.

Surface characterization techniques

SEM/EDS

Scanning electron microscopy (SEM) was used to study the surface morphology of the samples. The SEM analyses were performed with a Zeiss Ultra 55 field emission gun scanning electron microscope (FEG-SEM) equipped with an Oxford Instruments Inca energy dispersive X-ray spectroscopy (EDS). Imaging was performed by using the secondary electron detector (SEI-mode). All EDS analyses where performed by using an accelerating voltage of 20 kV of the primary electrons.

ToF-SIMS

All time-of-flight secondary ion mass spectrometry (ToF-SIMS) analyses were performed with a PHI TRIFT II instrument using a 15 keV pulsed liquid metal ion source isotopically enriched in ^{69}Ga. In this system, the secondary ions are accelerated up to ~3 keV before being deflected by 270° by three electrostatic hemispherical analyzers. Both positive and negative spectra were obtained using a 600 pA d.c. primary ion beam pulsed with a frequency of 8 kHz (m/z=0.5–1850 amu), a pulse width of 18 ns (~1 ns bunched) and rastered over a surface area of 100×100 μm^2. The mass resolution at mass +28 amu (Si^+) was around m/Δm=1900. All spectra were carefully calibrated using the exact masses of peaks of known composition such as $^7Li^+$ (7.0160 amu), Na^+ (22.9898 amu), Al^+ (26.9815 amu), $^{58}Ni^+$ (57.9353 amu) etc. Peak identification was done on the basis of the exact mass of the secondary ions.

Appendix 3

Results and discussion

SEM/EDS

Figures 1 and 2 show that there exist different types of particles in the fuel and ash powders. The SEM images show that all particle types have different surface morphology and the EDS spectra, Figs 3 and 4, show that the chemistry also differs between the particles. Thus, it can be expected that the results from the ToF-SIMS measurements can vary depending on which type of particle that is analyzed. Note that Li cannot be detected using EDS.

ToF-SIMS

The positive ToF-SIMS spectrum in Fig. 5 shows the mass spectrum from the surface of the carbon adhesive sticker that the powder is mounted on. The most abundant peaks are characteristic of a dimethyl siloxane type of polymer. Some of the characteristic peaks are due to a linear or cyclic structure:

Linear type:

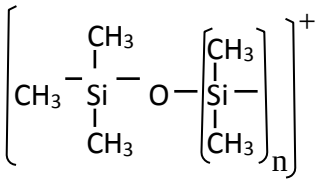

n	0	1	2	3
m/z	73	147	221	295

Cyclic type:

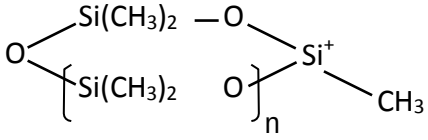

n	0	1	2	3
m/z	133	207	281	355

In Fig. 6 is the positive mass spectrum from a fuel powder particle shown. Except from peaks from elements such as Li (m/z = 7) and Ni (m/z = 58) it can be seen that the characteristic peaks from a siloxane is present in the mass spectra. To remove the siloxane that has diffused over the particle surface the area being analyzed is sputtered. Figure 7 show the positive mass spectrum from a particle surface sputter cleaned for 180 seconds. As can be seen, the characteristic peaks from the siloxane are more or less removed. The presence of a small Si peak, not seen in the figure, is the only remains of the siloxane. It should be noted that it cannot be excluded that the Si signal is due to an element coming from the fuel material itself. To prove that the siloxane is coming from the siloxane in the carbon adhesive sticker the sample were left for 16 hours in the vacuum chamber and analyzed at the same position that previously were sputter cleaned. The positive mass spectrum from this experiment is shown in Fig. 8 and the presence of the characteristic peaks from a siloxane is obvious, i.e. surface diffusion of the siloxane has occurred. Thus, all spectrum presented henceforth is acquired from sputter cleaned areas.

In Fig. 9 is the positive mass spectrum from the fuel and the ash presented. The main ion peaks are Li^+ (m/z = 6 and 7), Na^+ (m/z = 23), Ni^+ (m/z = 58 and 60 in the fuel and m/z = 62 in the ash) and 69^+ (m/z = 69). The Na^+ ion signal comes from the primary ions. The origin of Na^+ is either from some contamination, the carbon adhesive sticker or the material itself. Anyway, the probability for generating Na^+ as secondary ions is extremely high and the importance of the signal can be overestimated. The most interesting features is seen in the spectra from the ash where there seem to be a change in abundance of the isotopes for Li and Ni. In the fuel the abundance is close to what is naturally expected, see Table 1. In the ash the abundance of Li and Ni is altered, see table 1.

Appendix 3

Table 1. Measured and natural occurring abundances for Li and Ni ions in fuel and ash, respectively.

Ion	Fuel		Ash		
	Counts in peak	Measured abundance [%]	Counts in peak	Measured abundance [%]	Natural abundance [%]
$^{6}Li^{+}$	15804	8.6	569302	92.1	7.5
$^{7}Li^{+}$	168919	91.4	48687	7.9	92.5
$^{58}Ni^{+}$	93392	67	1128	0.8	68.1
$^{60}Ni^{+}$	36690	26.3	635	0.5	26.2
$^{61}Ni^{+}$	2606	1.9	~0	0	1.8
$^{62}Ni^{+}$	5379	3.9	133272	98.7	3.6
$^{64}Ni^{+}$	1331	1	~0	0	0.9

Figure 10 and 11 shows the positive mass spectra from different types of fuel and ash powder grains, respectively. Thus, as expected from the EDS analysis the appearance of the ToF-SIMS spectra will differ depending on particle analyzed.

Conclusions

The main conclusion that can be drawn from this SEM/EDS and ToF-SIMS study of powder samples from a fuel and a reaction product of the fuel, called ash, are:

- there are different types of powder particles in both samples.
- in the fuel sample, the detected ions has a natural abundance.
- In the ash sample, some ions, i.e. Li and Ni have an abundance deviating from the natural abundance.

Appendix 3

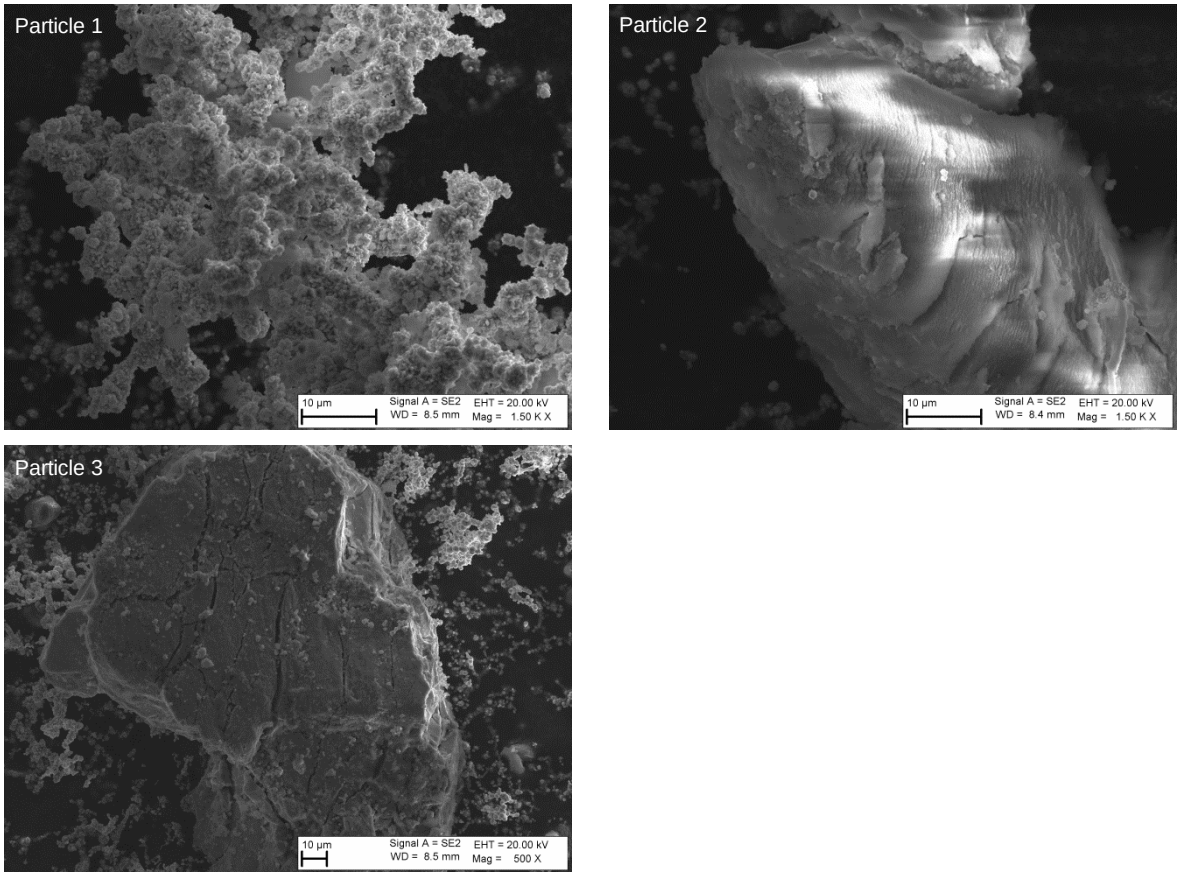

Figure 1. Three different types of particles from the fuel material.

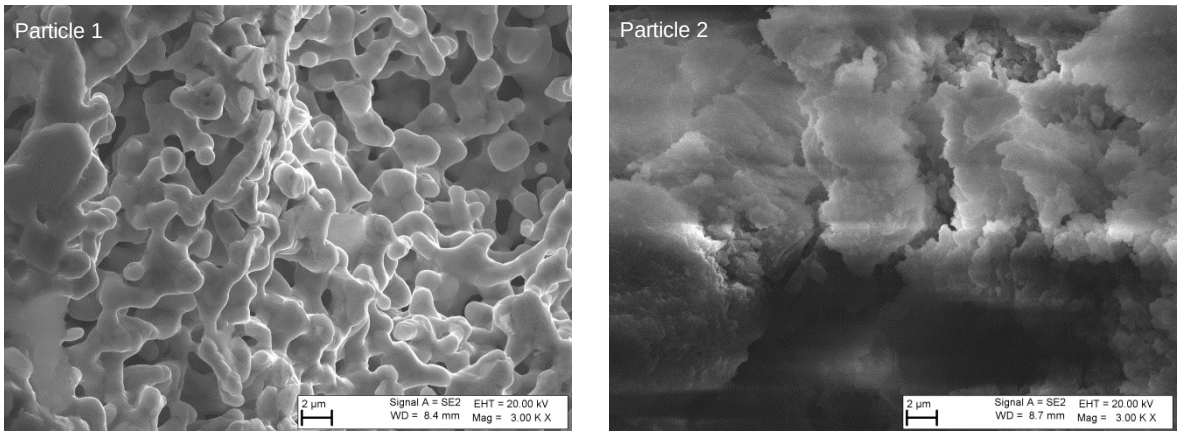

Figure 2. SEI of two different types of particles from the ash material.

Appendix 3

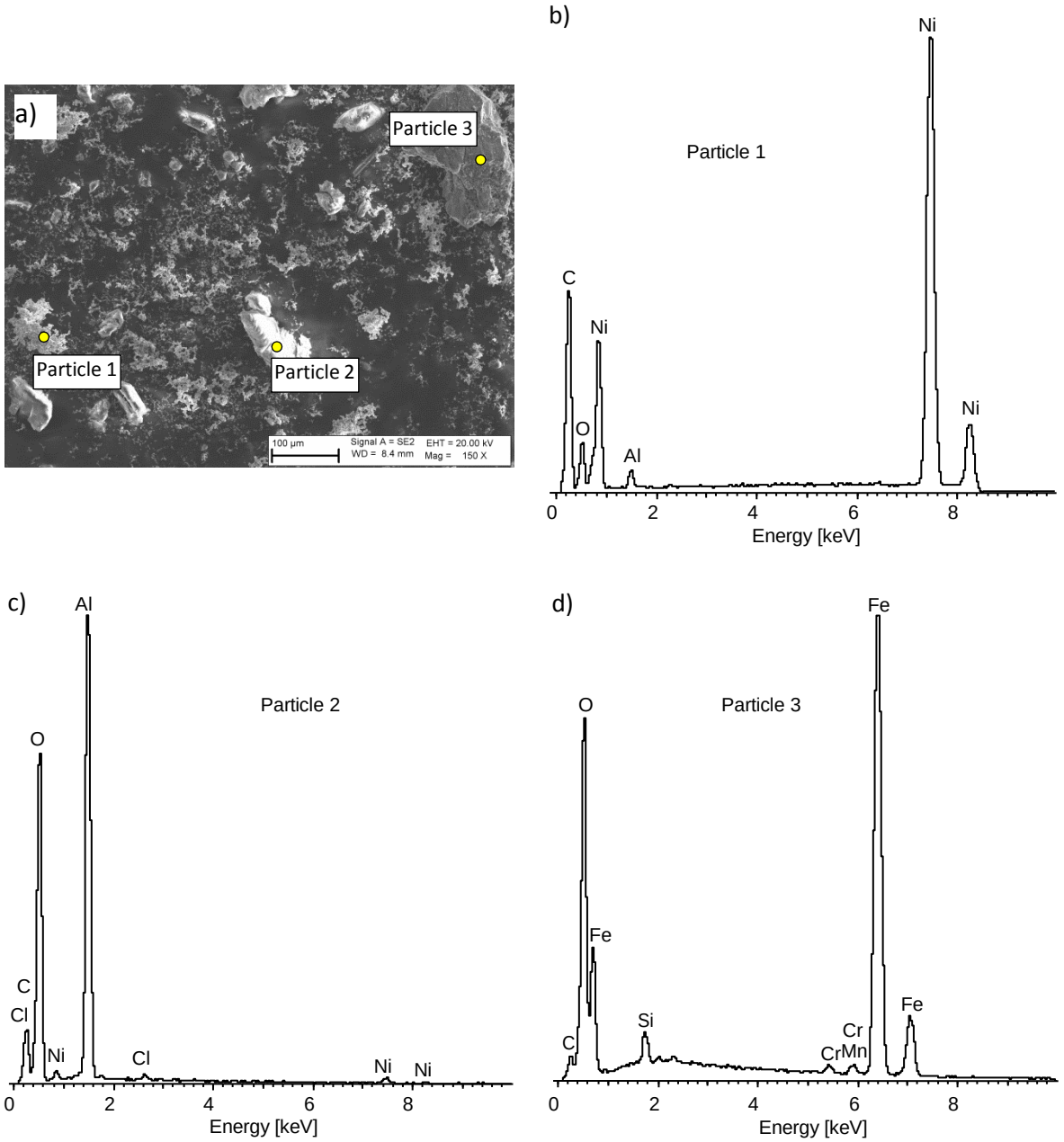

Figure 3. SEI showing the areas where EDS analysis where performed on the different fuel particles (a), EDS spectrum from the three different type of particles found in the fuel material; particle 1 (b), particle 2 (c) and particle 3 (d).

Appendix 3

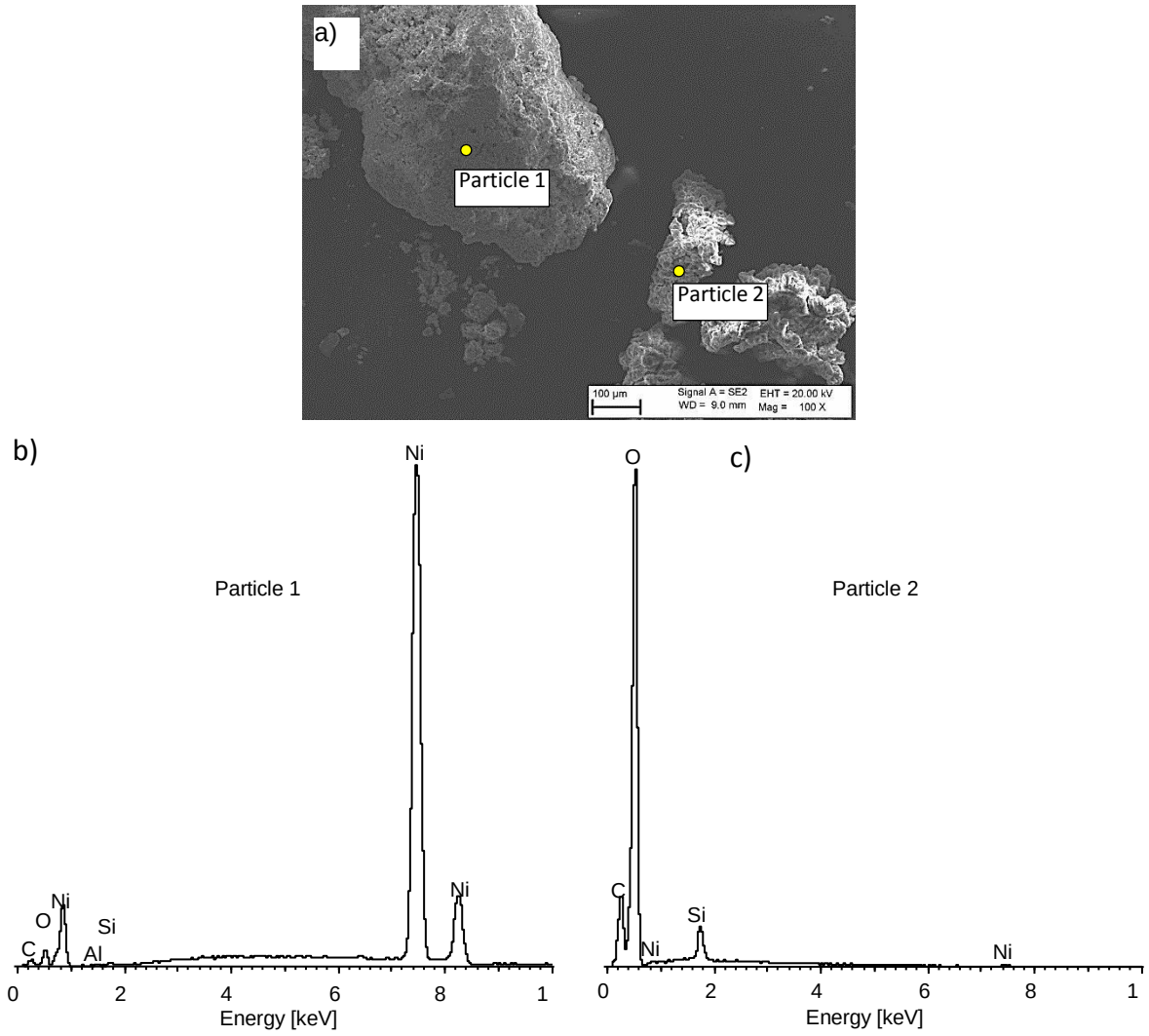

Figure 4. SEI showing the areas where EDS analysis where performed on the different ash particles (a), EDS spectrum from the two different type of particles found in the ash material; particle 1 (b) and particle 2 (c).

Appendix 3

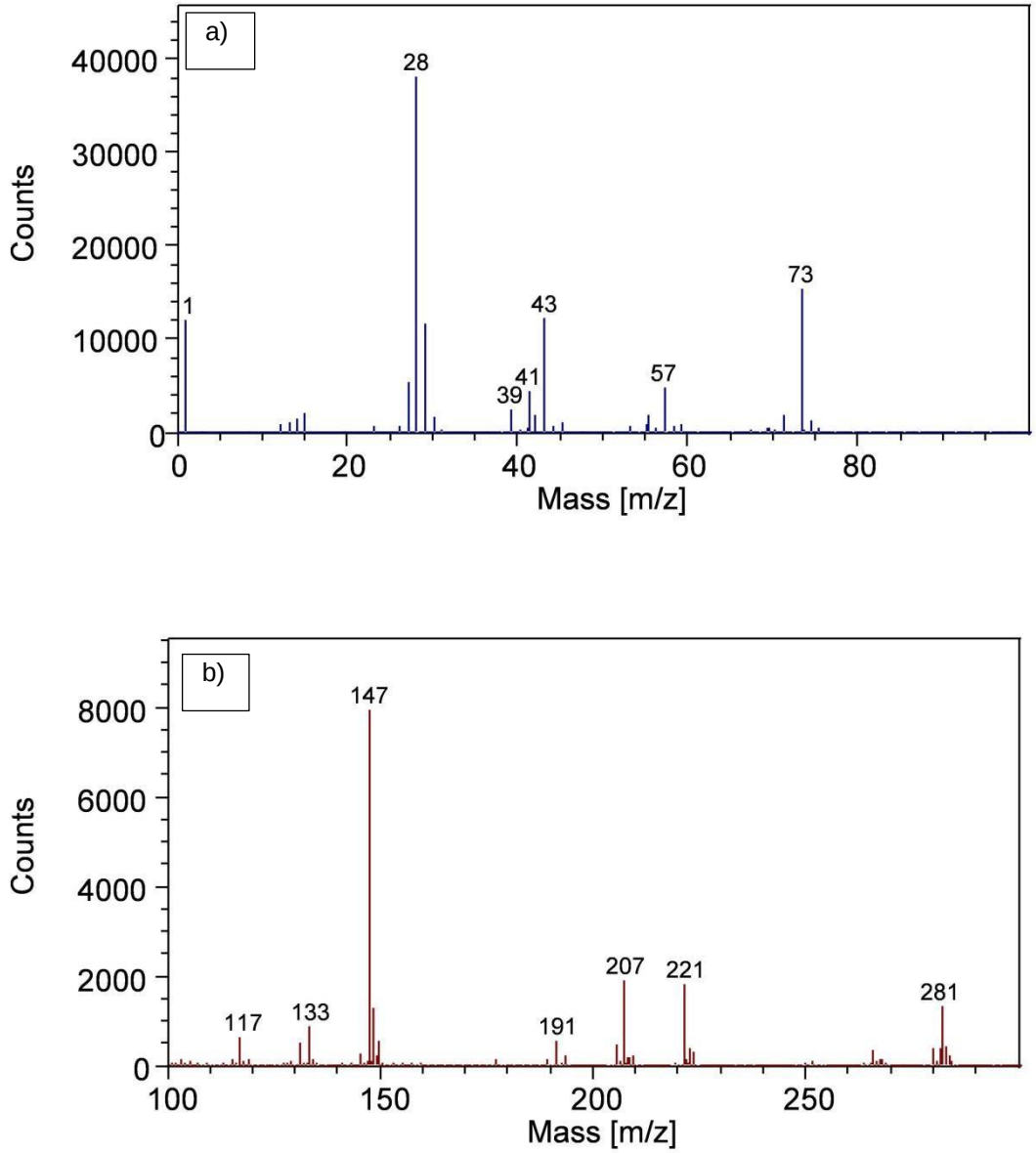

Figure 5. Positive ToF-SIMS spectrum of a carbon adhesive sticker surface: a) 0-100 amu b) 100-300 amu.

Appendix 3

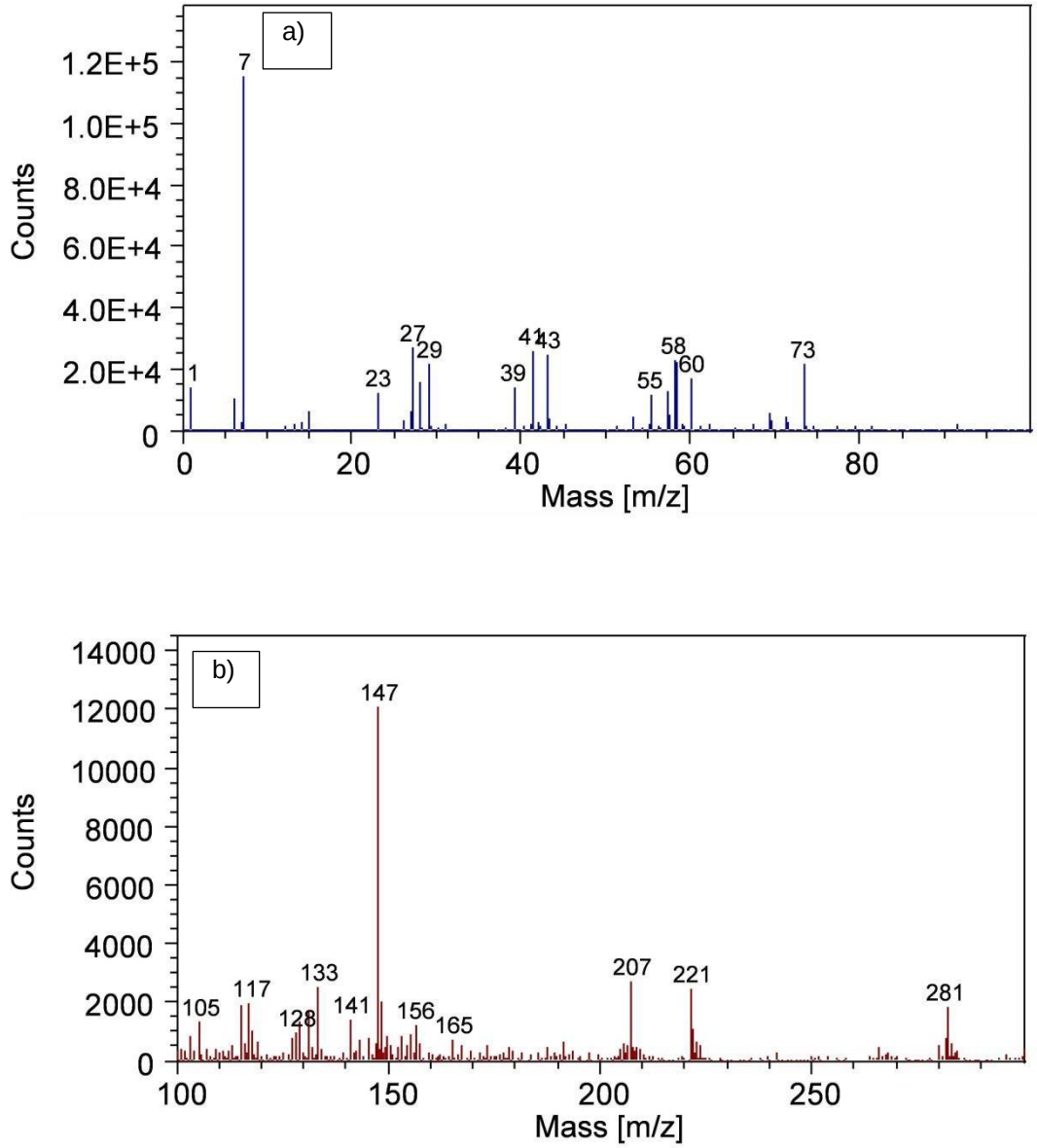

Figure 6. Positive ToF-SIMS spectrum of the surface of a fuel powder grain before sputter cleaning: a) 0-100 amu and b) 100-300 amu.

Appendix 3

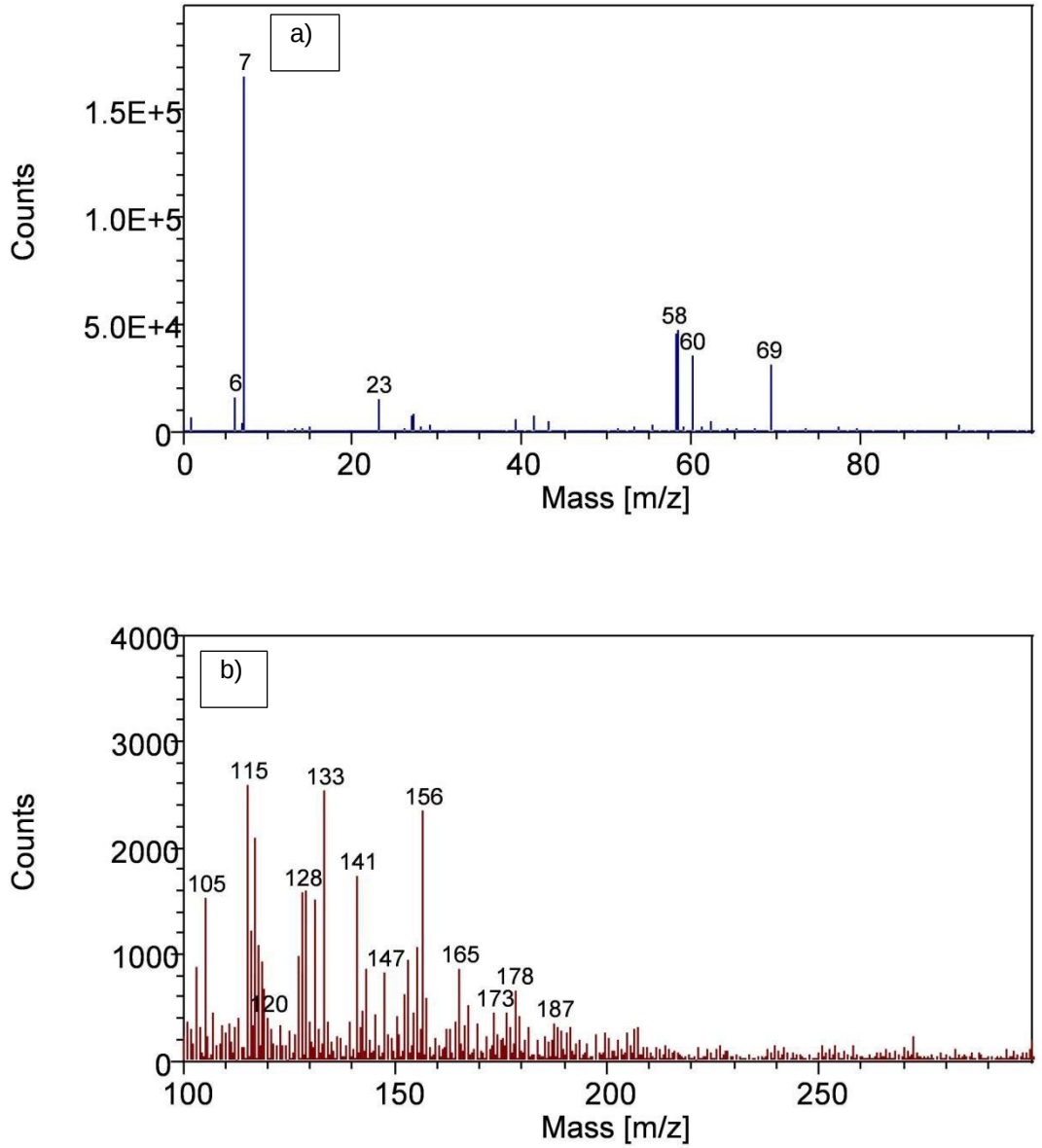

Figure 7. Positive ToF-SIMS spectrum of the surface of a fuel powder grain after sputter cleaning for 180 s: a) 0-100 amu and b) 100-300 amu.

Appendix 3

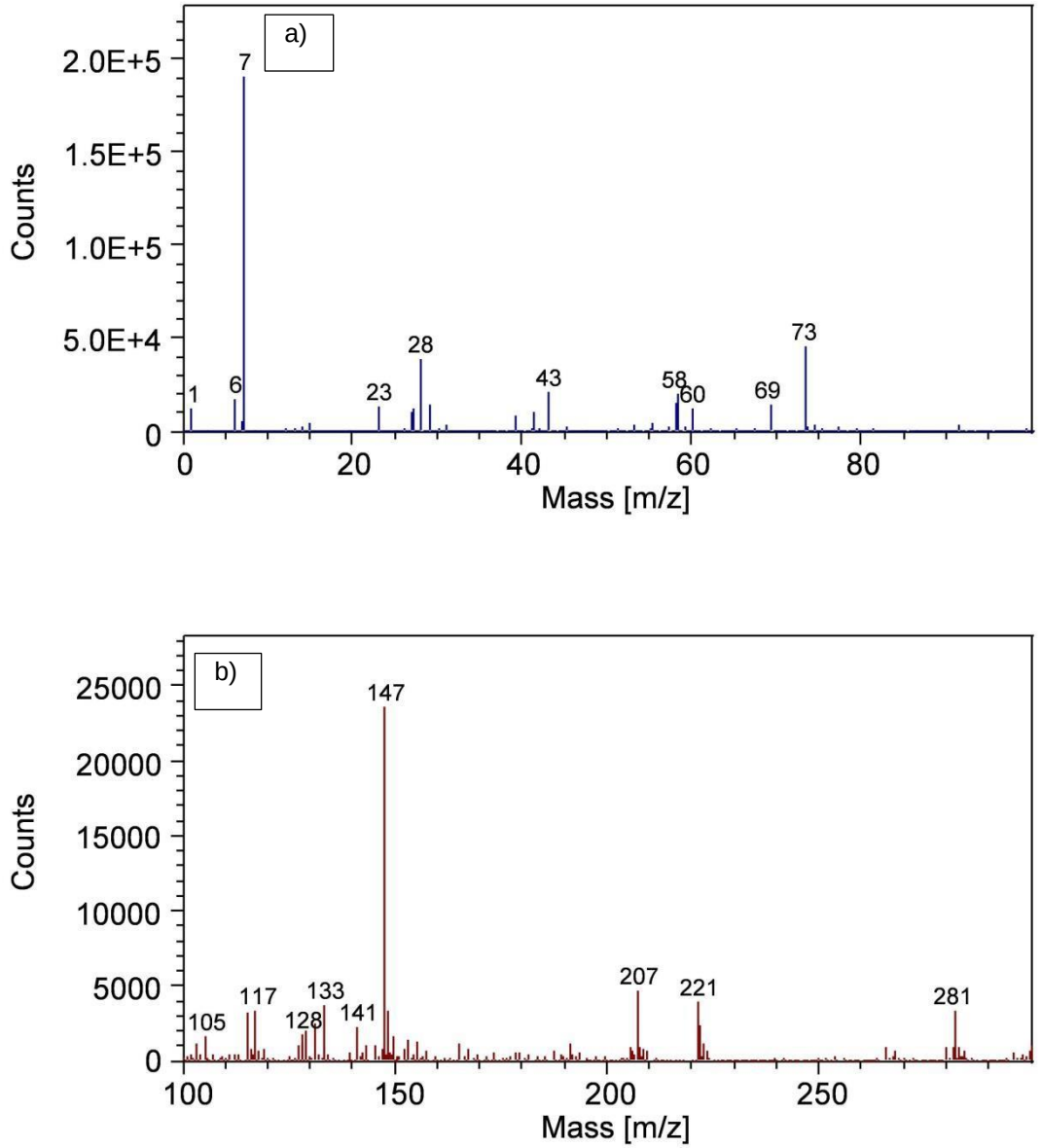

Figure 8. Positive ToF-SIMS spectrum of the surface of a fuel powder grain after sputter cleaning for 180 s followed by storing 16 h in the vacuum chamber: a) 0-100 amu and b) 100-300 amu.

Appendix 3

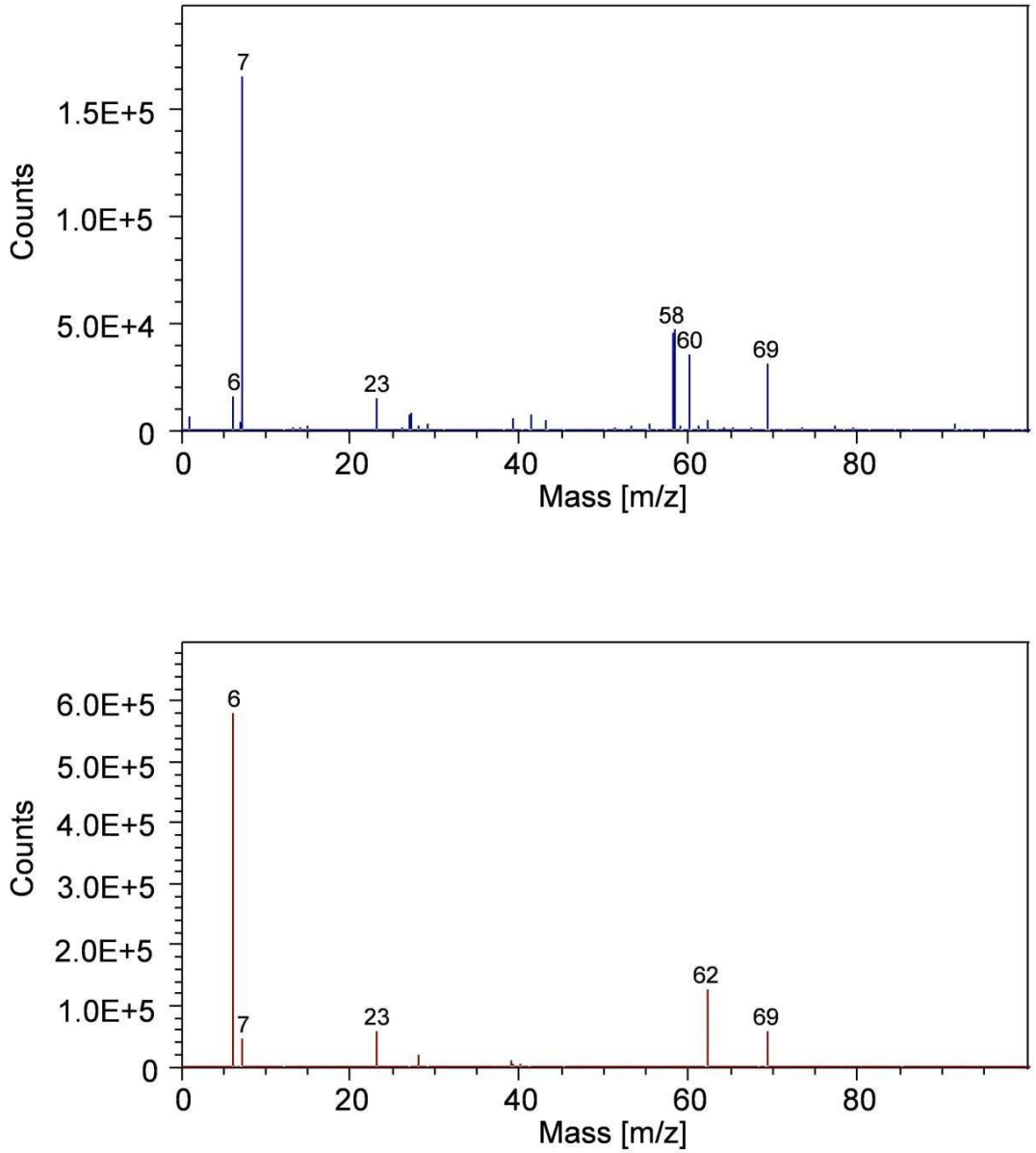

Figure 9. Positive ToF-SIMS spectrum of the surface of a fuel (above) and ash (below) powder grain after sputter cleaning for 180 s.

Appendix 3

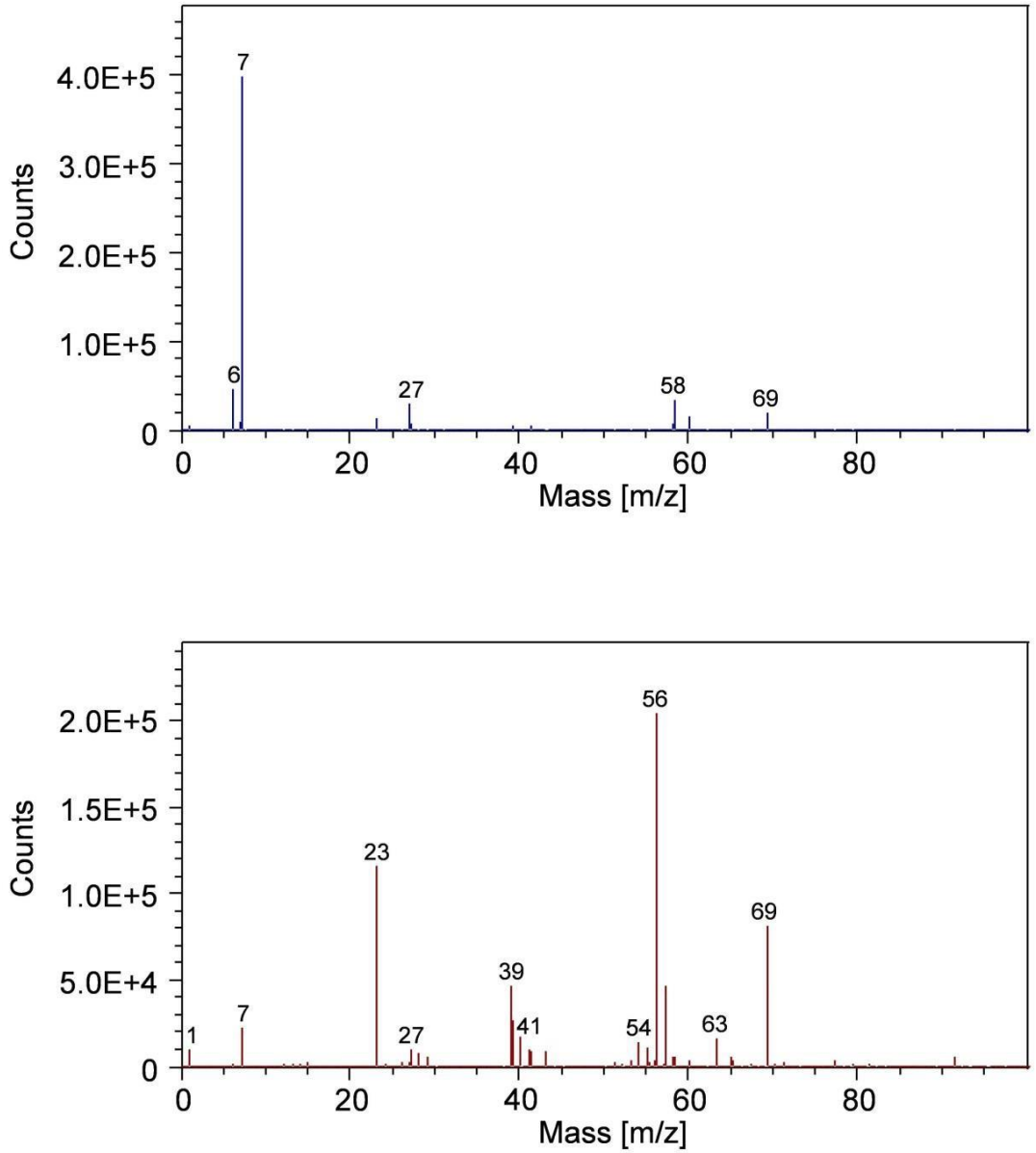

Figure 10. Positive ToF-SIMS spectrum of the surface of different types of fuel powder grains; one with low Ni content (above) and one rich in Fe (below) after sputter cleaning for 180 s.

Appendix 3

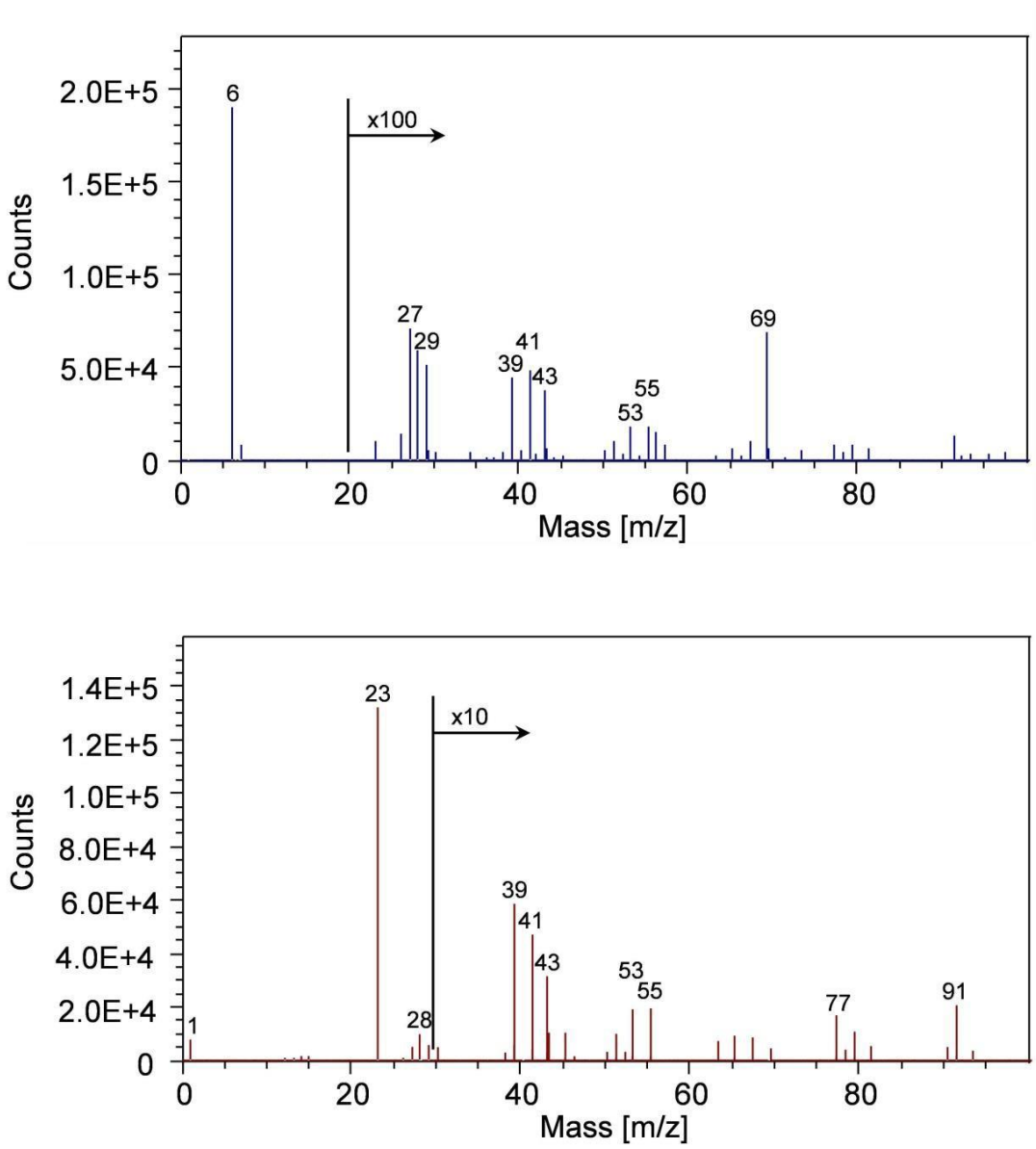

Figure 11. Positive ToF-SIMS spectrum of the surface of different types of ash powder grains; one with Li (above) and one without Li (below) after sputter cleaning for 180 s.

Appendix 4

Results ECAT ICP-MS and ICP-AES

Jean Pettersson
Inst. of Chemistry-BMC, Analytical Chemistry
Uppsala University

The samples are placed in quartz micro-Kjedahl vessels for dissolution with extra pure sub-boiled nitric acid (3.0 ml). They were heated to 136 degree and after that diluted to 50.0 ml.
Further dilution 1000 times was done before the measurement with ICP-MS.
The resulting values are corrected with blanks (the pure acid). The isotopic abundances are calculated and presented in the table below. Standards are known reference solutions in order to cheek the instrument. The natural isotopic abundance is shown in the last line of the table. The difference between the standards and the natural abundance is due to the fact that the signals are not mass biased corrected with isotopic reference standards.

mg sample	Sample id	Li 6	Li 7	Ni 58	Ni 60	Ni 61	Ni 62
	Standard 2	6,0	94,0	66,0	27,6	1,3	4,0
	Standard 3	6,0	94,0	66,1	27,5	1,3	4,1
	Standard 4	6,0	94,0	66,0	27,5	1,2	4,1
2,13	sample 1 ash	57,5	42,5	0,3	0,3	0,0	99,3
2,13	Sample 2 fuel	5,9	94,1	65,9	27,6	1,3	4,2
	Nat. abundance	7,6	92,4	68,1	26,2	1,1	3,6

Three different samples were analyzed by inductively coupled plasma atomic emission spectroscopy operated at standard conditions, ICP-AES.
The samples are placed in quartz micro-Kjedahl vessels for dissolution with extra pure sub-boiled nitric acid (3.0 ml). Heated to 136 degree and after that diluted to 50.0 ml.
The concentrations are calculated against acid matched calibration solutions.

The measured analytes were Ni, Li, and Al. The elements Ni and Al are measured with two independent emission lines to minimize risk for systematic errors. The elements C, H, O, N, He, Ar and F cannot be measured quantitatively by this technique.
Sample 1 was ash coming from the reactor in Lugano. Only a few granules of grey sample were possible to obtain from the ash and they didn't look exactly the same. One large and two very small granules were observed.
Sample 2 was the fuel used to charge the E-Cat. It's in the form of a very fine powder. Besides the analyzed elements it has been found that the fuel also contains rather high concentrations of C, Ca, Cl, Fe, Mg, Mn and these are not found in the ash.

Results as weight present of the samples.

	Ni 231nm %	Ni 232nm %	Li 670nm %	Al 396nm %	Al 394nm %
1 ash 2,13mg 50ml	95.9	95.6	0.03	0.00	0.05
2 fuel 2.13 mg 50ml	55.4	55.0	1.17	4.36	4.39